Spring 2008

Electromagnetic modeling of distributed coaxial cable crack sensors in reinforced concrete members

Mei Wang

Department:

ELECTROMAGNETIC MODELING OF DISTRIBUTED COAXIAL CABLE CRACK SENSORS IN REINFORCED CONCRETE MEMBERS

by

MEI WANG

A THESIS

Presented to the Faculty of the Graduate School of the

MISSOURI UNIVERSITY OF SCIENCE AND TECHNOLOGY

In Partial Fulfillment of the Requirements for the Degree

MASTER OF SCIENCE IN CIVIL ENGINEERING

2008

APPROVED BY

Genda Chen, Advisor
Marina Koledintseva
David Pommerenke

ABSTRACT

Distributed crack sensors were recently developed with coaxial cables that are composed of inner and outer conductors as well as dielectric layer in between. These sensors were designed based on the change in topology of the cable outer conductor structure under strain effects. Various tests of reinforced concrete (RC) beams and columns indicated that the newly designed sensors are 10~50 times more sensitive than commercial cables to the longitudinal elongation applied on their cable structures. The spatial resolution of the sensors is approximately 50 mm. Limited numerical simulations with the transmission line theory and the finite difference time domain model were performed to understand the general behavior of coaxial cable sensors.

The objectives of this study are (a) to develop an analytical solution of the reflection coefficient for a coaxial cable with one or more apertures, (b) to validate the analytical solution with the test data of commercial cables, and (c) to apply the analytical solution into cable sensors that were embedded in simply-supported RC beams in order to relate the aperture effect to the cracks in RC members. An emphasis will be placed on the effect of the geometry of apertures on the sensitivity and spatial resolution of a cable sensor as well as the effect of cable-concrete interface properties. Both simulations and test results consistently indicated that the reflection coefficient due to an aperture on a coaxial cable mainly depends on the length of the aperture that is projected to the cross sectional plane of the cable. The simulation results are in good agreement with the test data.

ACKNOWLEDGMENTS

I owe a great debt of gratitude to many people at the Missouri University of Science and Technology (formerly University of Missouri-Rolla), within the city of Rolla, and within my family. First I would like to express my deep appreciation to my advisor, Dr. Genda Chen. Dr. Chen was always available for advice and much needed guidance during my graduate study. Dr. Chen gave me this opportunity to work on an interdisciplinary project and provided resources to complete the challenging task. Dr. Marina Koledintseva and David Pommerenke were also a great source for guidance throughout my thesis project.

I am also grateful to Joseph Bishop, Brian Wood, Igor Izyumin and Taraka Ravi Shankar Mullapudi for their help during my study. I would like to thank my parents and family as well as my husband's family for all of their encouragement and support. I would like to thank my son, William and my daughter, Sarah who have been my motive for studying and working. The last but certainly not the least, I would like to thank my husband, Jianming, who has endured as much, if not more hardship during my quest to fulfill my requirements for a Master of Science in Civil Engineering.

TABLE OF CONTENTS

Page

LIST OF ILLUSTRATIONS

1. INTRODUCTION

1.1. GENERAL

Reinforced concrete (RC) members are widely used in buildings and civil infrastructures. Even under service loading, RC members often experience micro or hairline cracks. Additional cracking or strain induced by overstressing is of concern to engineers and the general public since it can degrade the performance of the structures or even affect the structural stability. Therefore, it is important to measure the strain in reinforcement or detect the significant crack in concrete to understand the actual behavior of RC structures and, more importantly, to prevent structures from collapsing.

Cracks are more concerned during the service life of RC structures due to their appearance, and associated water leakage and rebar corrosion. Excessive cracking of the concrete that covers the reinforcement is of particular interest. In this case, cracks will expose the reinforcement to the atmosphere, and subject it to continuing deterioration by corrosion. Therefore, a non-destructive technology that can be used to detect the location and width of cracks in RC members plays an important role in ensuring the structural safety, minimizing the maintenance cost and extending the service life. Recently developed distributed cable sensors (Chen et al., 2004) can aid in the detection of cracks in concrete. When embedded into any RC structural member, these sensors can identify the location and size of multiple concrete cracks, which can be an indication to the level of damages that the structural member has experienced. Previous works on this topic concerning the development and characterization of cable sensors were done by Huimin Mu (2003), Ryan McDaniel (2004) and Michael Brower (2007) at Missouri University of Science and Technology (formerly the University of Missouri–Rolla or UMR).

1.2. RESEARCH SIGNIFICANCE

The overall research in coaxial cable sensors, once proven, will enable engineers to detect cracks in RC structures with one or few coaxial cables in an affordable way. These sensors are extremely rugged; they also function as signal carrier without requiring external power cords. These attributes will eventually make the sensors uniquely suitable for applications in a harsh concrete construction environment. Cable sensors have a unique "memory" feature, which will make them a top choice for post-earthquake assessment of structural condition since the sensors can memorize the worst damage scenario during an earthquake without being connected to a data acquisition. The damage data can be retrieved from the sensors immediately after the earthquake event.

For this particular study, the main contribution is to develop a simulation tool that allows us to investigate the effects of cable geometries and cable-concrete interface properties on the sensitivity and spatial resolution of cable sensors. When a crack occurs at one location of a concrete member, the cable-concrete interface may locally experience a sudden change that is related to the slippage effect. Since this local effect is confined into such a small area, it would be a challenge to understand the effect by experiment. Simulation appears to be a viable alternative to tackle this problem after the boundary conditions of a model have been validated with some test data. Such effort will result in a viable tool for the optimization of distributed crack sensors.

1.3. RESEARCH OBJECTIVES

The objectives of this study are (a) to develop an analytical solution of the reflection coefficient for a coaxial cable with one or more apertures, (b) to validate the

analytical solution with the test data of commercial cables, and (c) to apply the analytical solution into cable sensors that were embedded in simply-supported RC beams in order to relate the aperture effect to the cracks in RC members. An emphasis will be placed on the effect of the geometry of apertures on the sensitivity and spatial resolution of a cable sensor as well as the effect of cable-concrete interface properties. The relation between crack width in the beams and reflection coefficient of the sensors embedded in beams will be evaluated.

2. LITERATURE REVIEW

2.1. GENERAL

The fundamental principle of cable sensors that have been designed and tested at Missouri University of Science and Technology (Missouri S&T) are electrical time/frequency-domain reflectometry (ETDR/EFDR). ETDR cable sensors utilize a transmission line as a signal carrier and a sensing unit is a pulse sampling technique that characterizes the distributed electrical properties of transmission lines. A time-domain reflectometer (TDR) launches low amplitude, high frequency pulses onto a transmission line (the cable under test) and then sequentially samples the reflected signal amplitudes. Typically, the reflected pulse amplitudes are displaced on a calibrated time scale. In this way, the change and discontinuity in cable impedance can be spatially located and assessed. Based on this principle, ETDR can be used as a remote electromagnetic sensor to determine the location and nature of various reflectors. The principle of the ETDR strain sensor is based on the transformation from mechanical strain to the characteristic properties of a transmission line.

2.2. USES OF ETDR IN GEOTECHNICS

ETDR is a measurement tool that has a variety of applications in electrical engineering and geotechnical engineering. It can be used as a remote electromagnetic sensor to determine the location and nature of various reflectors. Since the 1950s, ETDR has been applied by the power and telecommunication industries to locate and identify faults in transmission cables. The technology slowly began to develop some applications in geotechnics in the 1970s. More recently, its applications have been extended to various

topics including the characterization of solute transport parameters (Vanclooster et al., 1993), monitoring of abandoned mines (O'Connor et al., 1997), determination of the volumetric water content of soils in triaxial testing (Grozic et al., 2000), and identification of the causes of ground penetration radar reflections (Vanclooster et al., 1993). Monitoring of deformations in rock and soils can also be conducted using ETDR methods. A sensor can be grouted between shear zones allowing for deformation in the sensor at the shear zone interface. A study of the relationship between reflected TDR signals and the appearance of the diesel concentration in unsaturated soils was conducted by Chenaf et al. (2001). A state-of-the-art review by Benson and Bosscher (1999) and the book entitled "Geomeasurement by Pulsing TDR Cables and Probes" by O'Connor and Dowding (1999) summarized the many development in geo-applications. Several doctoral dissertations documented most of the original works (Su, 1987; Pierce, 1998).

2.3. USES OF ETDR IN STRUCTURS

The use of ETDR in geotechnical applications has been in effect since the 1970's. However, the use of ETDR for detecting structural damage is a relatively newer concept. In the application of crack detection, the sensors must exhibit a significantly greater sensitivity to stimuli since the desired threshold of detection is much smaller than that in shear zone detection of rock and soil. At present, its application is limited to reinforced concrete (RC) structures. Specifically, transmission cables are embedded into concrete specimens and, as continuous sensors, they are able to measure the change of characteristic impedance due to an external mechanical disturbance. Calibrated to

measure actual damage in structures, the change in impedance can be used as a damage indicator.

Commercially available coaxial cables have been embedded into concrete members for the purpose of crack detection by Su (1997) and Lin et al. (1998). Since these commercially available coaxial cables exhibited a very low sensitivity to cracking, Lin et al. (2000) proposed a new design of sensor involving the use of rubber as a dielectric material. A comparison study of more new sensor designs was conducted by Mu (2003). The TDR sensors developed at Missouri S&T were previously validated by Mu (2003), McDaniel (2004), and Brower (2007). Based on their investigations, it was concluded that the new sensor designs resulted in the improved sensitivity of coaxial cable sensors by 10~50 times, enabling their use in structural engineering.

ETDR sensors have also been studied in post-tensioning ducts for the detection of voids, corrosion, and wet-grouted sections (Okanla et al., 1997). Other types of sensors have been used for crack detection as well. They are beyond the scope of this thesis and will not be discussed herein. The advantages and disadvantages of cable sensors and fiber optic sensors (with Brillioun Scattering Time-domain Reflectometry) were compared by Chen et al. (2006).

3. SENSOR DESIGN AND IMPLEMENTATION

3.1. GENERAL

As discussed in Section 2, ETDR is the process by which crack sensors are monitored for crack propagation. In order to achieve the signal generation and reflected wave sampling, a digital sampling oscilloscope is used. The oscilloscope uses an ETDR sampling head that sends a series of step pulses through the transmission line and then samples the reflected signal. The sampling device used in this study is a time-domain reflectometer (TDR).

In the event of an electrical discontinuity, part of the pulse is reflected back to the TDR. The electrical discontinuity creates a local change in the characteristic impedance of the transmission line. The digital oscilloscope is capable of measuring the voltage of the reflected wave and by measuring the time it takes for the signal to return to the source, the distance to that discontinuity can be extrapolated. As a result, the coefficient of reflection from that discontinuity can be determined. Eq. (1) shows the relationship between the reflected wave voltage (V_o^-) and the pulse signal voltage (V_o^+) which is also defined by the ratio of characteristic impedances of the two locations in question. This would be the unaffected sensor impedance (Z_o) and the impedance looking into the defected cable (Z), respectively.

$$\Gamma = \frac{V_o^-}{V_o^+} = \frac{Z - Z_o}{Z + Z_o} \qquad (1)$$

A coaxial cable is essentially a pair of conductors with a dielectric material separating them. These two conductors provide a path for the current from the pulse signal to travel. As seen in Figure 3.1, there is an outer conductor and an inner conductor. As stated before, the reflected wave will appear when the impedance of the cable changes. An impedance change is caused by discontinuity in the signal carrier. This discontinuity is caused by some type of change or interruption in the path of the current, which is brought about by either a geometric change or by a change in topology of one of the conductors or by change of dielectric. In the case of the distributed crack sensors used in this study, the change in topology of the outer conductor is what causes an interruption of current flow at the location of a crack in the concrete. This enables the detection of the crack.

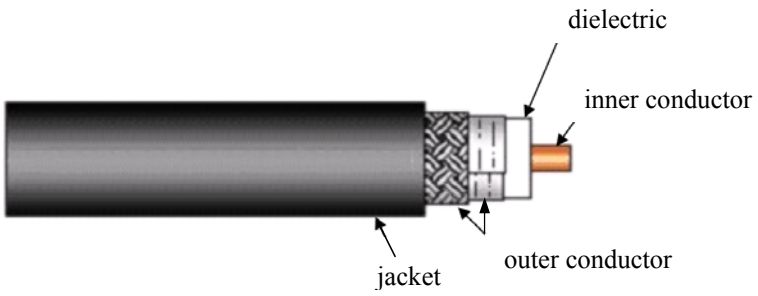

Figure 3.1 Typical Coaxial Cable

As discussed previously, this technique has been used to locate breaks in transmission lines for a number of years. In the case of crack detection, the sensor not only functions as a transmission line, it is also a sensing unit. In effect, the crack sensors are a modified version of coaxial cables. While it is desirable in most other applications of coaxial cables for the signal to remain uninterrupted, it is required in the design of the crack sensors for the signal to be altered as much as possible when the correct external

stimuli occurs, e.g. a crack in the concrete. This is achieved by allowing the outer conductor of the sensor to experience a change in topology at the location of a crack.

3.2. SENSOR TYPE

Several sensor designs were developed and tested by Mu (2003), McDaniel (2004) and Brower (2007). The type of sensors that will be used to validate the numerical model in this study consists of an inner core of 10-gage copper wire with a Teflon dielectric. The outer conductor of the sensor is a stainless steel spiral, wrapped around the Teflon dielectric as shown in Figure 3.2. To keep the edges of steel spirals in contact with each other, an adhesive conductive layer is placed over the spirals. When two adjacent steel spirals in the sensor separate, the outer conductor or steel spiral can slide over the smooth Teflon surface creating a discontinuity in the sensor. Figure 3.3 shows the effect of a partial separation on the flow of current.

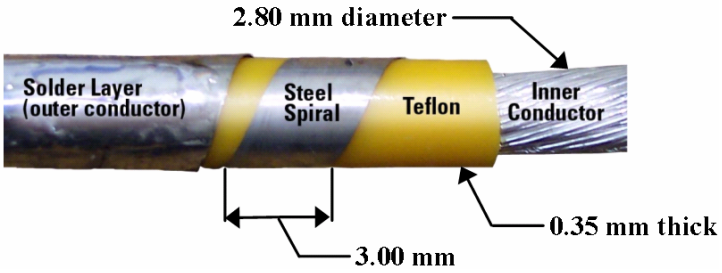

Figure 3.2 Cut-away of the Sensor

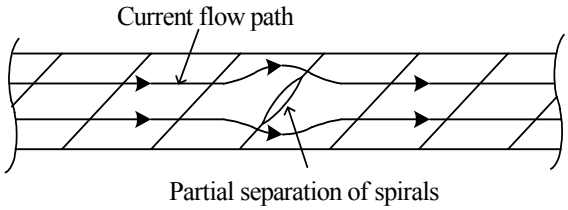

Figure 3.3 Path of Current along Disturbed Outer Conductor

4. SIMULATION OF DISTRIBUTED ETDR CRACK SENSOR

4.1. EQUIVALENT CIRCUIT MODEL OF THE ETDR STRAIN SENSOR

To gain more insight into how the prototype ETDR strain sensor responds to the longitudinal deformation, it is desirable to develop an analytical model using the transmission line theory. A lossless coaxial cable can be modeled as a series L-C-L structure as shown in Figure 4.1. Any configuration change on the cable's structure, for example, by separating two adjacent rounds of the spiral wrapping outer conductor, will introduce an extra inductance at the changing point in the transmission line. An extra capacitance will also be introduced but be neglected in this study due to its secondary effect. The equivalent circuit model of this configuration change is illustrated in Figure 4.2. The L_{gap} represents the extra inductance caused by the separation in the outer conductor. In the equivalent circuit model, this extra inductance acts like a lumped circuit element in the transmission line.

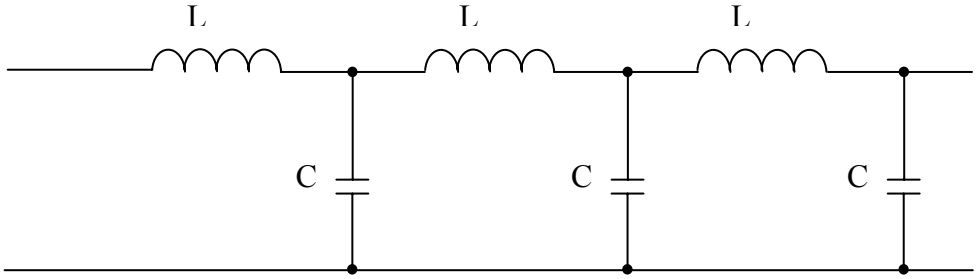

Figure 4.1 Equivalent Circuit of a Lossless Coaxial Cable

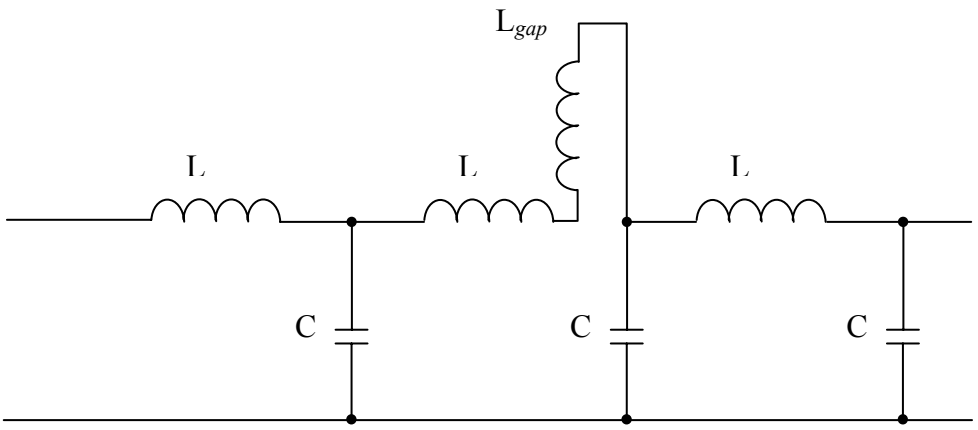

Figure 4.2 Equivalent Circuit of a Lossless Coaxial Cable with Configuration Change

The prototype ETDR crack sensor was designed based on the concept of the configuration change of the coaxial cable when the cable is strained longitudinally. The above discussions indicate that the configuration change is equivalent to an extra inductance at the deformation point in the transmission line. This leads to the change of impedance at the point and its corresponding reflection coefficient.

4.2. ELECTROMAGNETIC MODELING OF SHIELDED CABLES WITH SMALL APERTURES

ETDR technique is based on the application of a test signal to the cable input connection and analysis of the time history of the reflected signal to monitor the response of faults. From a theoretical point of view, when a pulse signal is used, the knowledge of the time delay, the shape and the amplitude of the reflected pulse allows us to determine the location and characteristics of the cable defects.

In this study, a coaxial cable with a small aperture is considered and the effect of the aperture on the pulse propagation in the cable is analyzed to evaluate the reflection

coefficient or reflected voltage. A simple yet accurate representation of the discontinuity developed by Cerri et al. (2005) is used in this study. The previous study by Cerri et al. (2005) was limited to a square shape of discontinuity; this study will extend the theory to studying defects of any shape.

The slot defect used in this study, whose electromagnetic characteristics were studied to determine its reflection coefficient, is an elliptical aperture on the cylindrical surface of a coaxial cable as shown in Figure 4.3. This type of defect on the cable does not modify considerably the wave propagation and the field distribution along the cable so that the analysis can be simplified.

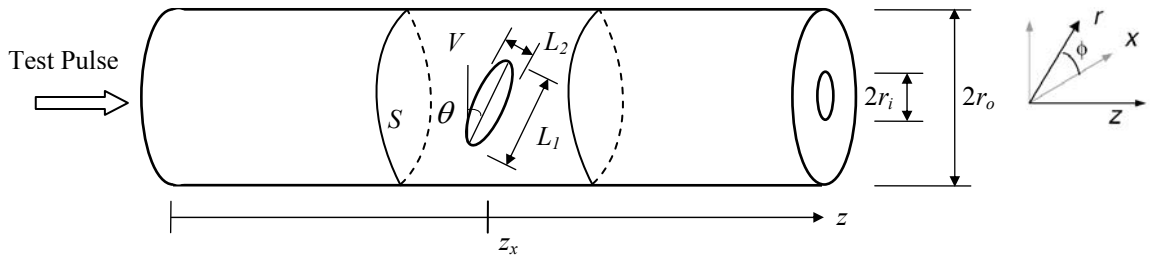

Figure 4.3 Geometry of Defects in the Shield of a Coaxial Cable

An electric dipole normal to the aperture and a magnetic dipole tangential to the aperture can be used to approximately represent the effect of a small aperture. The moments of the electric and magnetic dipoles are respectively related to the normal component of the exciting electric field and to the tangential component of the exciting magnetic field through the electric and magnetic polarisability that depends on the aperture dimension and shape. If the slot is small in comparison with wavelength, the undisturbed wave fields of the cable can be used for the calculation of dipole moments. In this case, let a Transverse Electromagnetic (TEM) wave propagate along the cable. The

electric dipole moment $\vec{P}$ and magnetic dipole moment $\vec{M}$ that represent the slot effect can then be expressed into:

$$\vec{P} = \varepsilon_0 \alpha_e \vec{E}_0(\vec{r}_s, z_x)\delta(\vec{r} - \vec{r}_s) \tag{1}$$

$$\vec{M} = \alpha_m \vec{H}_0(\vec{r}_s, z_x)\delta(\vec{r} - \vec{r}_s) \tag{2}$$

in which $(\vec{r}_s, z_x)$ is the coordinate of the center of the slot, ε_0 is the permittivity of vacuum, $\alpha_e = \dfrac{\pi L_1^3(1-e^2)}{3E(e)}$ is the electric polarisability of the aperture, $\alpha_m = \dfrac{\pi L_1^3 e^2}{3\,[K(e)-E(e)]}$ is the magnetic polarisability of the aperture, and $\vec{E}_0 = \dfrac{V_0 \hat{r}}{r \ln(r_o/r_i)} e^{-j\beta z}$, $\vec{H}_0 = \dfrac{I_0 \hat{\phi}}{2\pi r} e^{-j\beta z}$ are the electric and magnetic fields of the coaxial cable due to the incident TEM wave, respectively. Here $\hat{r}$ and $\hat{\phi}$ are the unit vectors in their respective directions. The quantities r_o and r_i are the outer and inner radius of the coaxial cable, respectively, as indicated in Figure 4.3. The quantities I_0 and V_0 are current and voltage on the outer shield, respectively; $e = \sqrt{1 - \left(\dfrac{L_2}{L_1}\right)^2}$ is the eccentricity of the ellipse; $K(e) = \dfrac{\pi}{2}\left(1 + \dfrac{e^2}{4}\right)$ and $E(e) = \dfrac{\pi}{2}\left(1 - \dfrac{e^2}{4}\right)$ are the incomplete integrals of the first and second kind. $\beta = \omega\sqrt{\varepsilon_0 \mu_0}\sqrt{\varepsilon_r} = \omega\sqrt{\varepsilon_r}/C_0$, $C_0 = 3 \times 10^8 m/s$ is the light speed in free space, ε_r is the relative permittivity of dielectric inside the cable.

Based on the Lorentz's reciprocity theorem, the two dipoles can then be coupled with the modes of the coaxial cable. Since $j\omega\vec{P}$ has the same role in Maxwell's equation

as impressed current $\vec{J}_e$ and $j\omega\mu_0\vec{M}$ has the same role as $\vec{J}_m$. Equivalent currents are defined as

$$\vec{J}_e = j\omega\vec{P} \tag{3}$$

$$\vec{J}_m = j\omega\mu_0\vec{M} \tag{4}$$

where ω is the angle frequency of the traveled wave, μ_0 is the permeability of vacuum.

Assume that $\vec{J}_e$ and $\vec{J}_m$ produce the electric and magnetic fields, $\vec{E}_1$ and $\vec{H}_1$. From Maxwell's equations,

$$\nabla\times\vec{E}_0 = -j\omega\mu\vec{H}_0 \tag{5a}$$

$$\nabla\times\vec{H}_0 = -j\omega\mu\vec{E}_0 \tag{5b}$$

$$\nabla\times\vec{E}_1 = -j\omega\mu\vec{H}_1 - \vec{J}_m \tag{6a}$$

$$\nabla\times\vec{H}_1 = -j\omega\mu\vec{E}_1 - \vec{J}_e \tag{6b}$$

where μ is the permeability of the dielectric. (5a) $\bullet\,\vec{H}_1$-(6b) $\bullet\,\vec{E}_0$+(5b) $\bullet\,\vec{E}_1$-(6a) $\bullet\,\vec{H}_0$ gives

$$\nabla\bullet\left[\vec{E}_1\times\vec{H}_0\right] - \nabla\bullet\left[\vec{E}_0\times\vec{H}_1\right] = \vec{J}_e\bullet\vec{E}_0 - \vec{J}_m\bullet\vec{H}_0 \tag{7}$$

Integrating Eq. (7) over a small volume V of the coaxial around the aperture, and letting $\vec{E}_1 = \Gamma\vec{E}_0$ and $\vec{H}_1 = -\Gamma\vec{H}_0$, where Γ is the reflection coefficient, gives

$$2\Gamma\iint_S(\vec{E}_0\times\vec{H}_0)\bullet(-\hat{z})dS = \iiint_V(\vec{J}_e\bullet\vec{E}_0 - \vec{J}_m\bullet\vec{H}_0)dV \tag{8}$$

in which S is the left circular surface of V. The left hand side of Eq. (8) equals to $2\Gamma V_0 I_0$, or $2\Gamma\dfrac{V_0^{\,2}}{Z_0}$, where $Z_0 = \dfrac{\eta\ln(r_o/r_i)}{2\pi}$ is the characteristic impedance of the coaxial cable and

η is the characteristic impedance of the dielectric. The right hand side of Eq. (8) equals to $\vec{E}_0(\vec{r}_s, z_x)\bullet\vec{J}_e(\vec{r}_s) - \vec{H}_0(\vec{r}_s, z_x)\bullet\vec{J}_m(\vec{r}_s)$ since $\vec{J}_e$ and $\vec{J}_m$ are different from zero only in the center of the slot. It can also be written into $j\omega\vec{E}_0(\vec{r}_s, z_x)\bullet\vec{P} - j\omega\vec{H}_0(\vec{r}_s, z_x)\bullet\vec{M}$. Thus, the reflection coefficient can be expressed as a function of the modulus of both electrical and magnetic polarizability,

$$\Gamma = \frac{(\mu_0 M - \eta P) j\omega}{4V_0 \pi r_o \ln(r_o / r_i)} e^{2j\beta z_x} \tag{9}$$

The modulus of the reflection coefficient is

$$|\Gamma| = \frac{(\mu_0 M - \eta P)\omega}{4V_0 \pi r_o \ln(r_o / r_i)} \tag{10}$$

Finally, the reflected voltage can be expressed into:

$$V_{refl}(f) = \frac{(\mu_0 M - \eta P) j\omega}{4\pi r_o \ln(r_o / r_i)} e^{2j\beta z_x} \tag{11}$$

In the equivalent circuit model, the reflection coefficient can be expressed by the characteristic impedance as

$$\Gamma = \frac{Z_{c0} - Z_0}{Z_{c0} + Z_0} \tag{12}$$

where Z_{c0} is the characteristic impedance of defected transmission line, and Z_0 is the characteristic impedance along the uniform line. In frequency domain, Z_{c0} can be expressed into

$$Z_{c0} = Z_0 + j\omega L_{gap} \tag{9}$$

from which L_{gap} can be evaluated numerically after the reflection coefficient has been determined.

4.3. RESULTS AND DISCUSSIONS

Following is a presentation of numerical results based on the electromagnetic model discussed in Section 4.2. These results are presented in the form of reflection coefficients in frequency domain and in the form of the time history of the reflected voltages when a Gaussian test pulse is used.

4.3.1. Single Non-inclined Aperture. Consider a coaxial cable with an elliptical aperture that is located at 0.2 m from the beginning of the cable where the cable is connected to a TDR. The major axis of the elliptical aperture, perpendicular to the direction of wave propagation, is L_1=3 mm long. The minor axis along the propagation direction is L_2=0.3 mm long. The outer radius of the cable is r_o=3.175 mm, the inner radius is r_i=0.605 mm, and the characteristic impedance is Z_0=50 Ohm. The test pulse, the reflected voltage and the reflection coefficient are shown in Figures 4.4-4.6, respectively.

It can be seen from Figures 4.4 and 4.5 that the amplitude of the reflected wave is approximately 300 times lower than that of the incident signal. Moreover, the shape of the reflected pulse is quite different from the incident one; it rather resembles the derivative of the incident wave. In particular, its sign shows the inductive nature of the discontinuity. It should also be noticed that the model accurately predicts the evolution of the response.

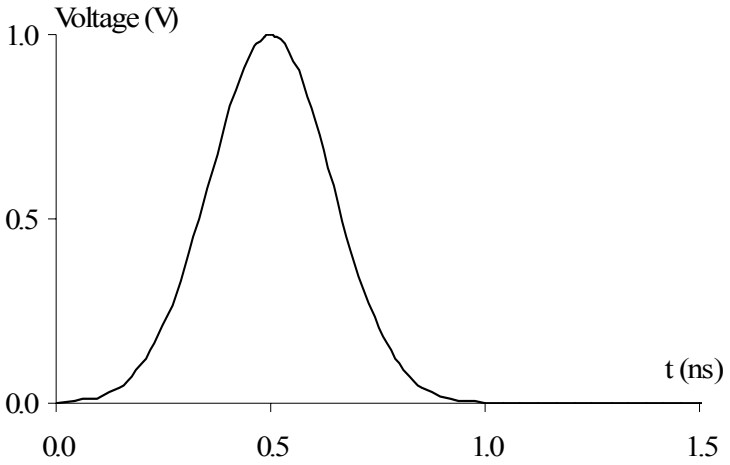

Figure 4.4 Gaussian (test) Pulse

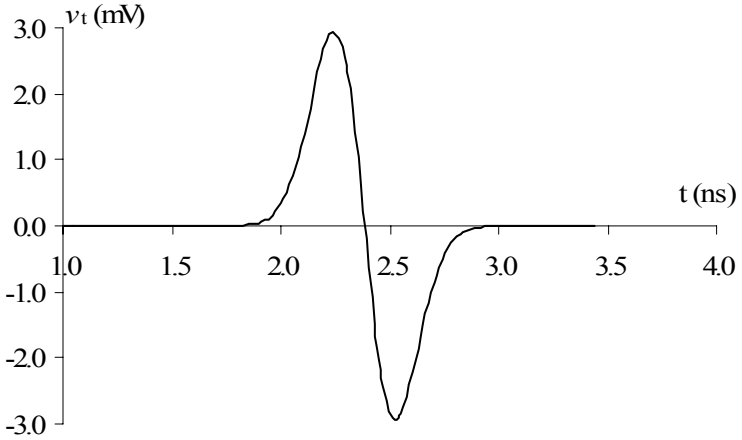

Figure 4.5 Reflected Voltage

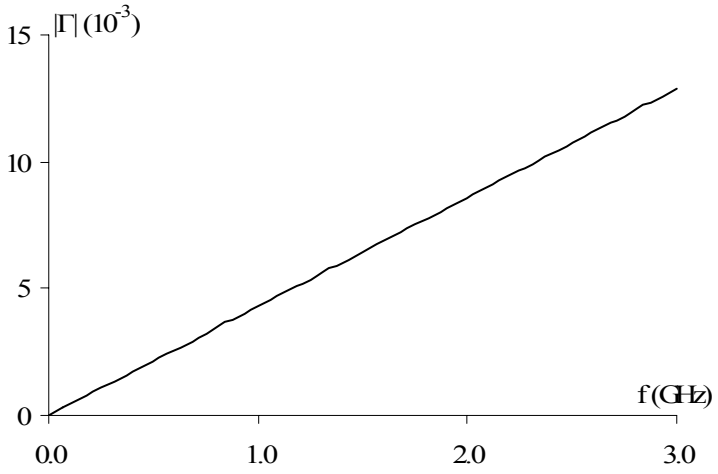

Figure 4.6 Reflection Coefficient Amplitude of the Aperture in the Coaxial Shield

Figures 4.7, 4.8 and 4.9 present the relations between the reflection coefficient and the major axis length of the aperture, the relation between the reflection coefficient and the frequency, and the relation between the reflection coefficient and time, respectively. Each figure covers three cases: Case (a) for L_1/L_2=10, Case (b) for L_2=0.2 mm and Case (c) for L_1=4 mm.

It can be seen from Figures 4.7-4.9 that the length of the aperture (perpendicular to the propagation direction) dominates the effect of the slot on the outer conductor of the coaxial cable. The width of the aperture (along the propagation direction) only affects the reflection coefficient slightly. The reflection coefficient even decreases slightly with increase of the aperture width due mainly to the simplification of the theoretical analysis.

4.3.2. Single Inclined Aperture. Consider the same case as described in Section 4.3.1 except that the aperture is inclined $\pi/4$ to the propagation direction. Figures 4.10, 4.11 and 4.12 show the relationship between the reflection coefficient / reflected voltage and the length/width of the aperture. The results are very similar to those of the non-inclined aperture. It can be seen that the length of the aperture still dominates. The width of the aperture slightly affects the reflection coefficient only.

Figure 4.13 presents the relationship between the reflection coefficient and the inclination angle, the reflection coefficient in frequency domain and the reflected voltage in time domain, respectively. It can be seen from Figure 4.13 that the reflected signal weakens as the angle increases.

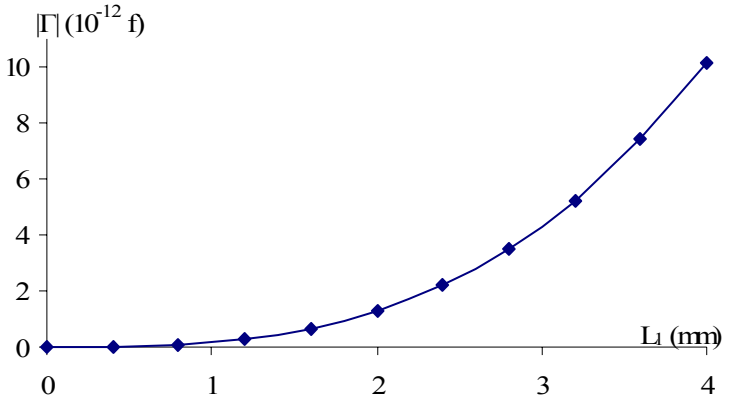

Case (a): varying L_1 and $L_1/L_2 = 10$

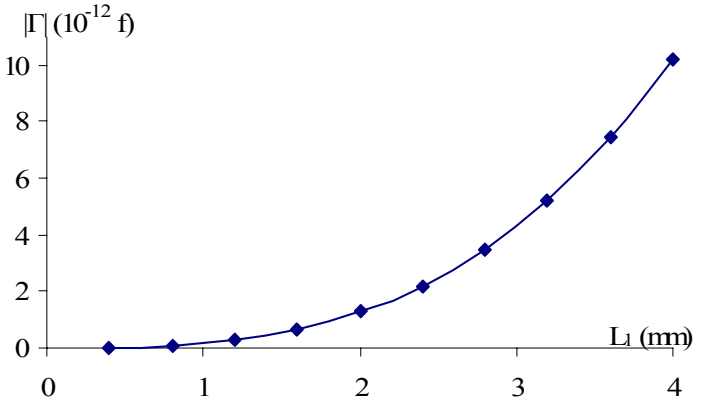

Case (b): varying L_1 and $L_2 = 0.2$ mm

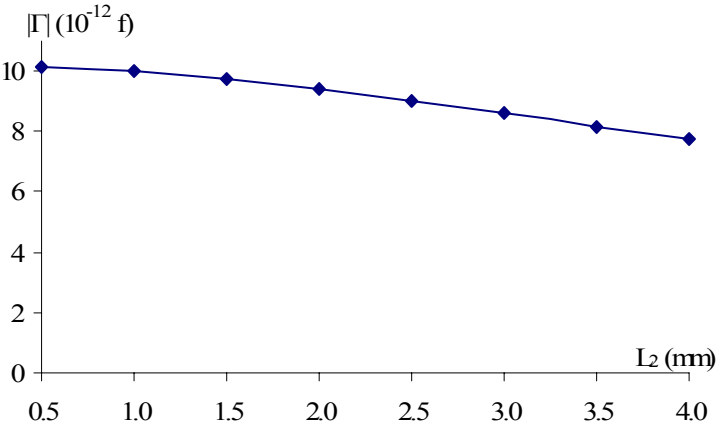

Case (c): $L_1 = 4$ mm and varying L_2

Figure 4.7 Reflection Coefficient vs. Aperture Dimension

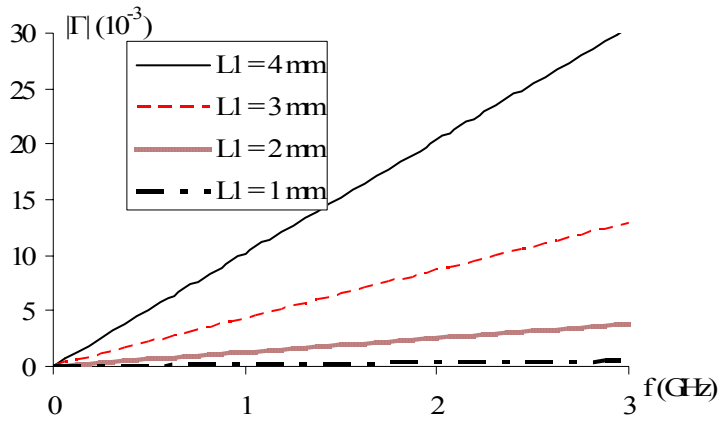

Case (a): $L_1/L_2 = 10$

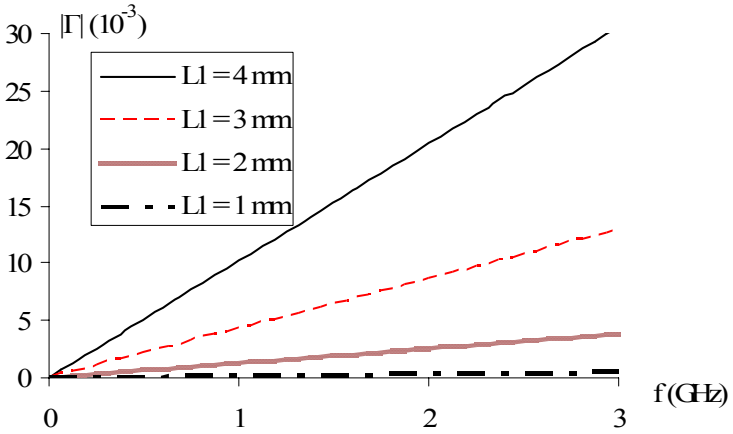

Case (b): $L_2 = 0.2$ mm

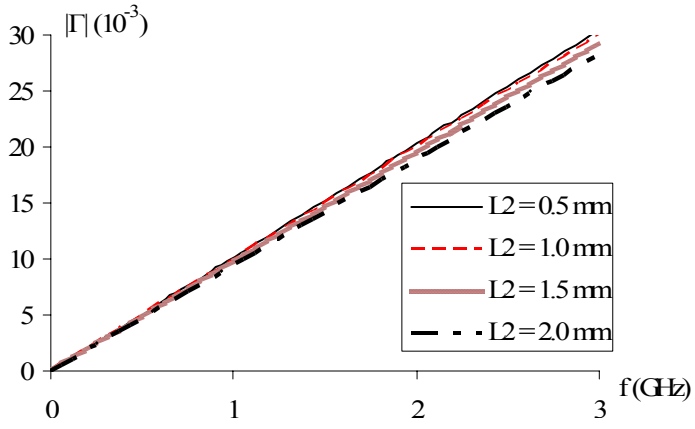

Case (c): $L_1 = 4$ mm

Figure 4.8 Reflection Coefficient vs. Frequency

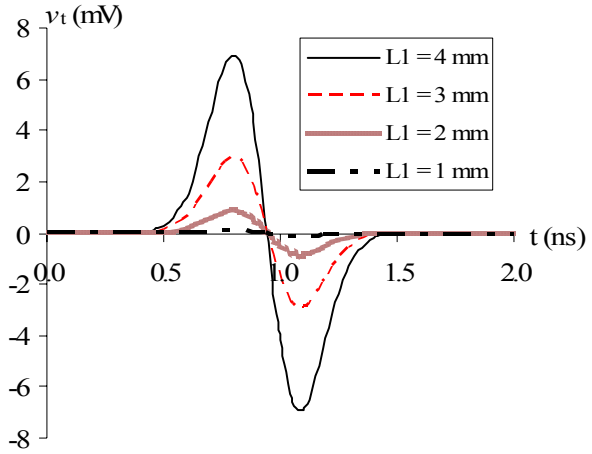

Case (a): $L_1/L_2 = 10$

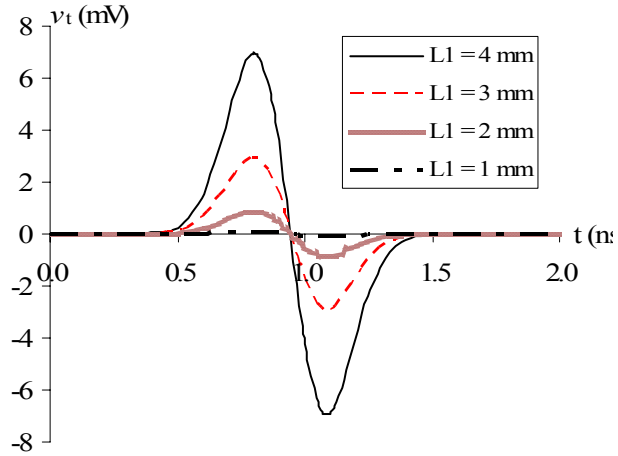

Case (b): $L_2 = 0.2$ mm

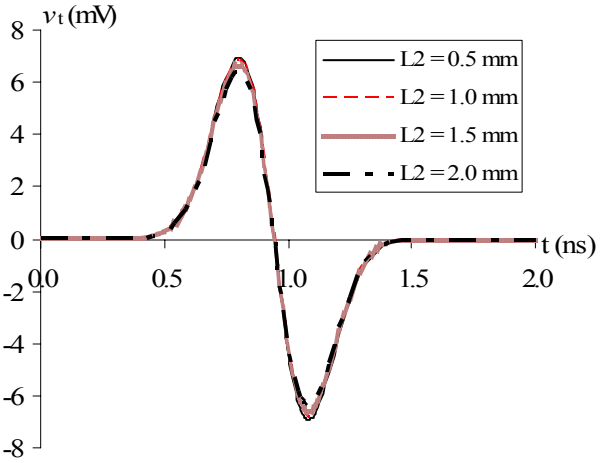

Case (c): $L_1 = 4$ mm

Figure 4.9 Reflected Voltage vs. Time

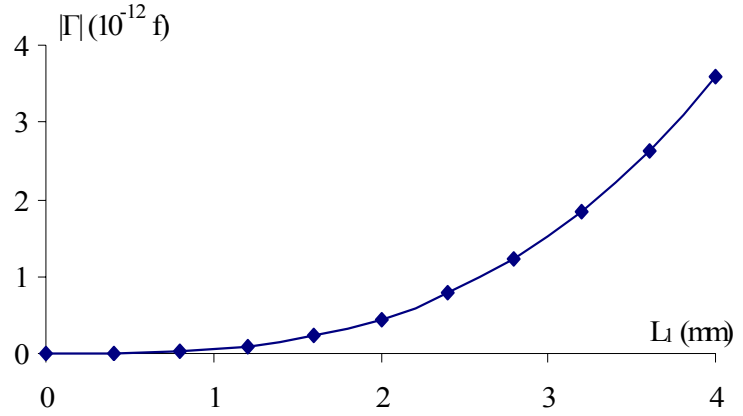

Case (a): varying L_1 and L_1/L_2 = 10

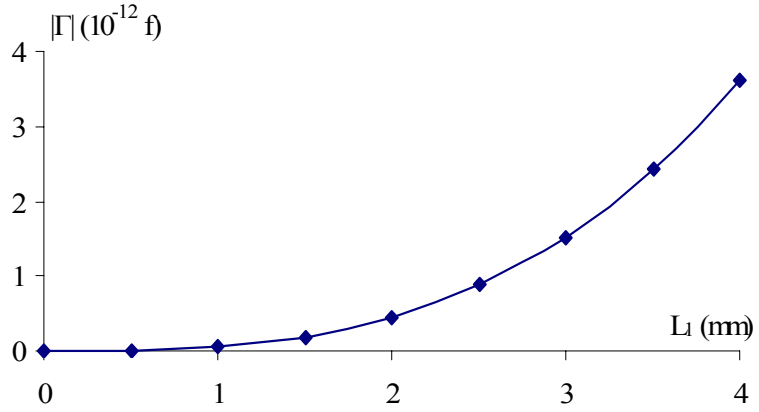

Case (b): varying L_1 and L_2 = 0.2 mm

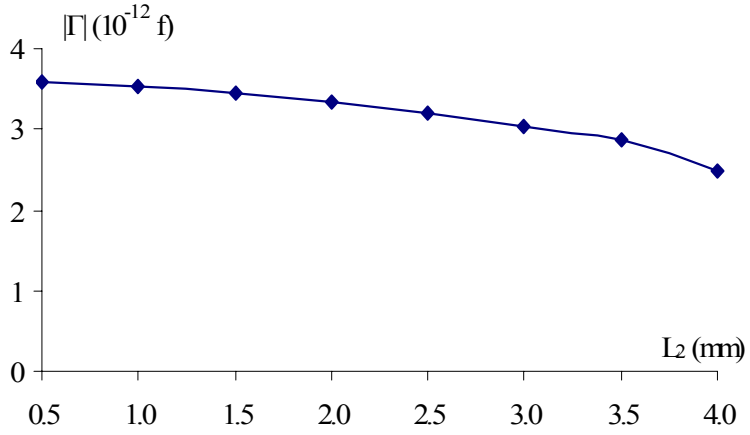

Case (c): L_1 = 4 mm and varying L_2

Figure 4.10 Reflection Coefficient vs. Aperture Dimension

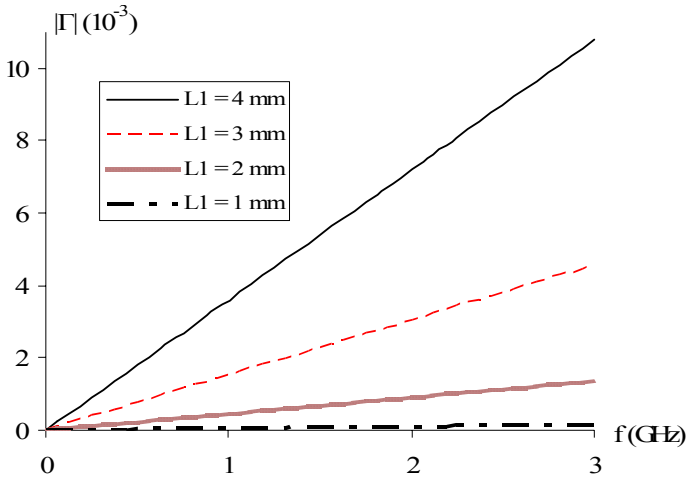

Case (a): $L_1/L_2 = 10$

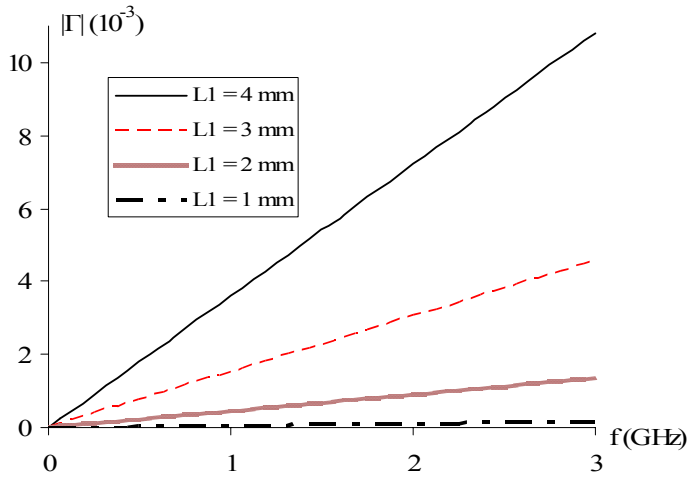

Case (b): $L_2 = 0.2$ mm

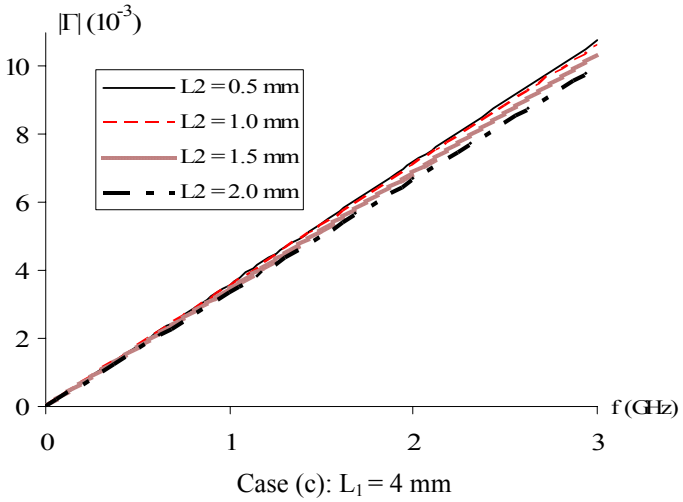

Case (c): $L_1 = 4$ mm

Figure 4.11 Reflection Coefficient vs. Frequency

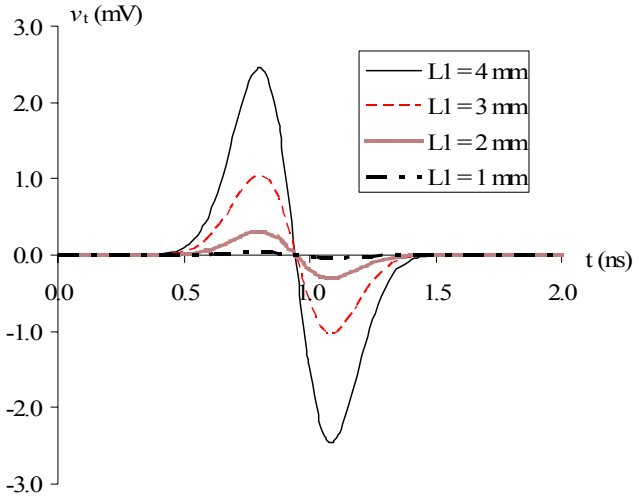

Case (a): $L_1 / L_2 = 10$

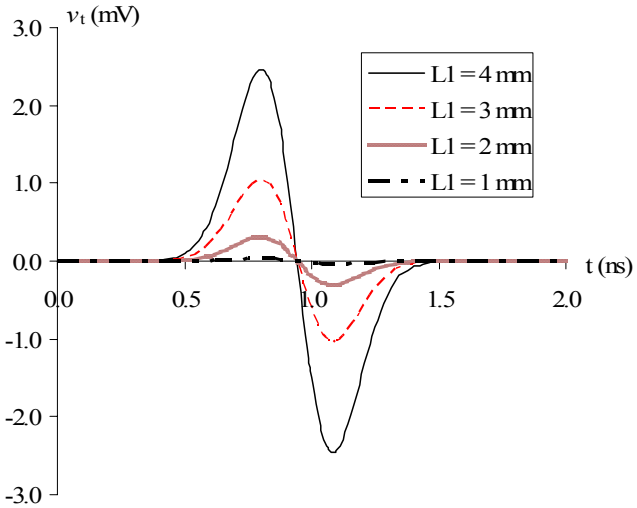

Case (b): $L_2 = 0.2$ mm

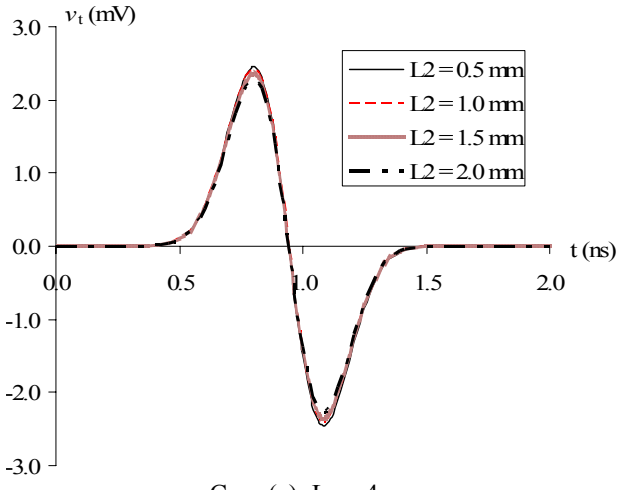

Case (c): $L_1 = 4$ mm

Figure 4.12 Reflected Voltage vs. Time

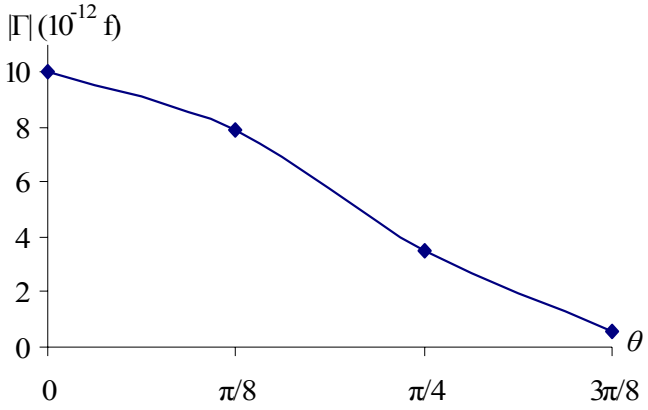

Case (a): Reflection Coefficient vs. Inclined Angle θ

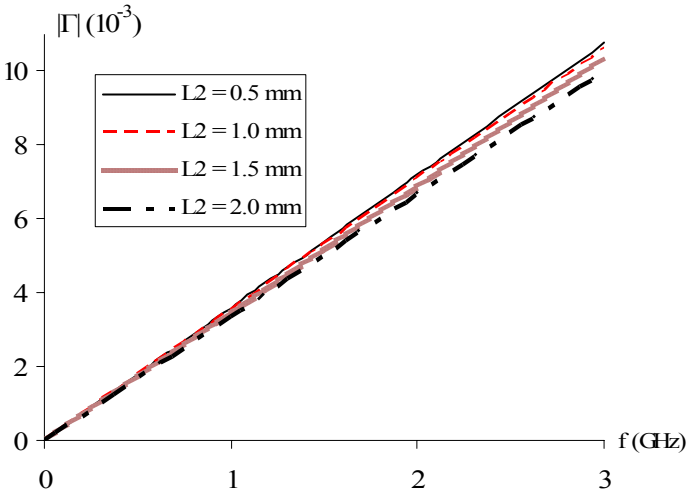

Case (b): Reflection Coefficient vs. Frequency

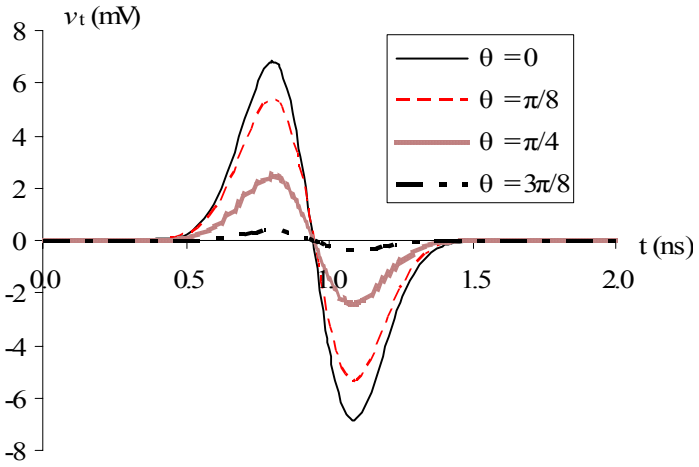

Case (c): Reflected Voltage vs. Time

Figure 4.13 Effect of the Inclination of the Aperture

4.3.3. Multiple Inclined Apertures. Consider two apertures located at 0.5 m and 1.0 m from the beginning of the cable, respectively. Figure 4.14 shows the reflected voltage in time domain. Both apertures are 0.2 mm wide, but the first aperture is 2 mm long and the second aperture is 4 mm long. The inclination angles of both apertures are $\pi/4$.

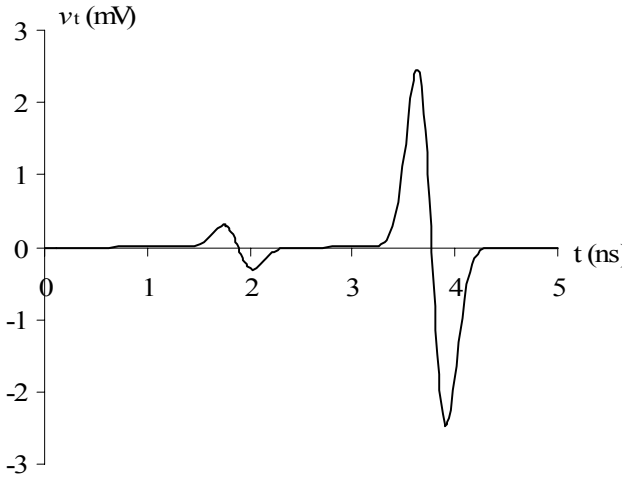

Figure 4.14 Reflected Voltage vs. Time (2 Slots Spacing at 0.5 m)

It can be observed from Figure 4.14 that the second waveform is identical to that presented in Figure 4.13(c) for $\theta = \pi/4$. It is also seen that the first waveform in Figure 4.14 is completely separated from the second waveform, indicating that the spatial resolution is less than 0.5 m. Further analysis with closer spacing (0.06 m) between the two apertures shows the change of peak reflection coefficient with the spacing in Figure 4.15. It can be seen that the spatial resolution for this particular case is approximately 0.06 m for peak interference less than 5%. Due to the separation of the two waveforms, however, conclusions similar to those due to a single aperture can be drawn for multiple apertures.

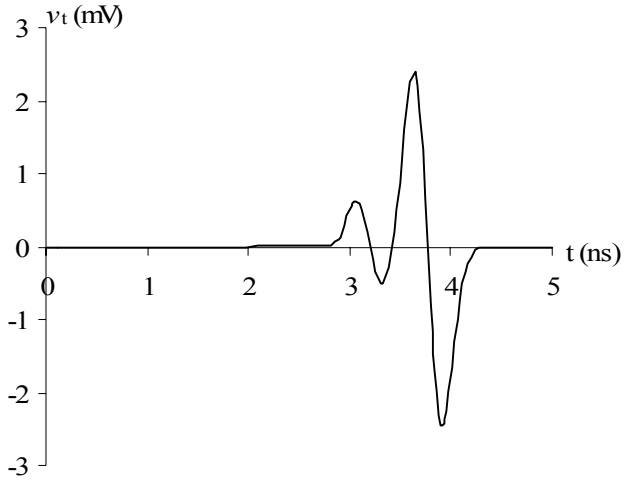

Figure 4.15 Reflected Voltage vs. Time (2 Slots Spacing at 0.06 m)

4.4. SUMMARY

An L-C-L model was built to simulate the ETDR sensor made of coaxial cables. A coaxial cable with small apertures was analyzed; the reflection coefficient and reflected voltage were evaluated. Based on the numerical simulations, the following conclusions can be drawn:

1) The reflected pulse resembles the derivative of an incident wave. In particular, its sign shows the inductive nature of the discontinuity as a result of an aperture.
2) The length of an aperture perpendicular to the propagation direction is a determining parameter. The width of the aperture is of secondary effect..
3) As the inclination angle of an aperture from the propagation direction increases, the reflected wave weakens.
4) The sensitivity of the sensor increases as aperture length increases. The reflected voltage waves from two slots that are larger than 0.06 m apart can be clearly identified individually, indicating that a spatial resolution of approximately 0.06 m can be achieved.

5. VALIDATION OF THE ELECTROMAGNETIC MODEL

5.1. INTRODUCTION

The electromagnetic model presented in Section 4 was validated by comparing its simulations with other theoretical results and experimental data at three levels. First, both theoretical analyses and measurements presented in Cerri et al. (2005) were used to understand the model capability for the details of reflected voltages in time domain under an idealized Gaussian pulse. Secondly, test data from two commercial coaxial cables with slots of various sizes and inclinations were used to further understand the model capability under a realistic step pulse.

5.2. COMPARISON WITH RESULTS OBTAINED BY CERRI ET AL. (2005)

5.2.1. Properties of the Tested Cable. Consider an RG213 coaxial cable, shown in Figure 5.1, with a 6mm×6mm square slot at 0.6 m from the beginning of the cable as illustrated in Figure 5.2. The outer diameter of the cable is 10.287 mm and the outer diameter of the core is 7.239 mm. The characteristic impedance of the cable is 50 Ohm. The Gaussian pulse used during tests was narrow and had a rise time of less than 0.5 ns.

Figure 5.1 Picture of the Coaxial Cable Tested (Cerri et al., 2005)

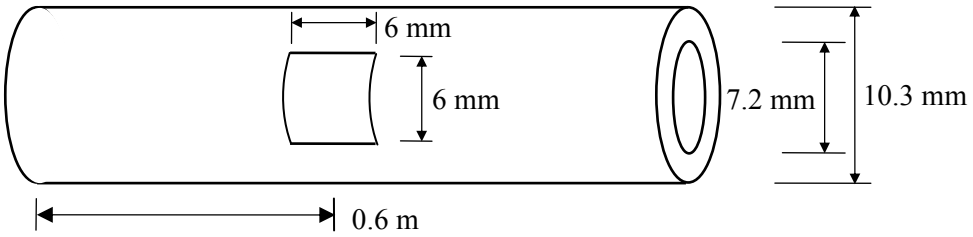

Figure 5.2. Geometry of the Slot on the Surface of Outer Conductor

5.2.2. Results. The reflected wave due to the presence of the slot is presented in Figure 5.3. In this figure, both theoretical and experimental results by Cerri et al. (2005) are reproduced. It can be observed that the analytical results from this study are in excellent agreement with the theoretical results by Cerri et al. (2005); they also coincide well with the experimental data.

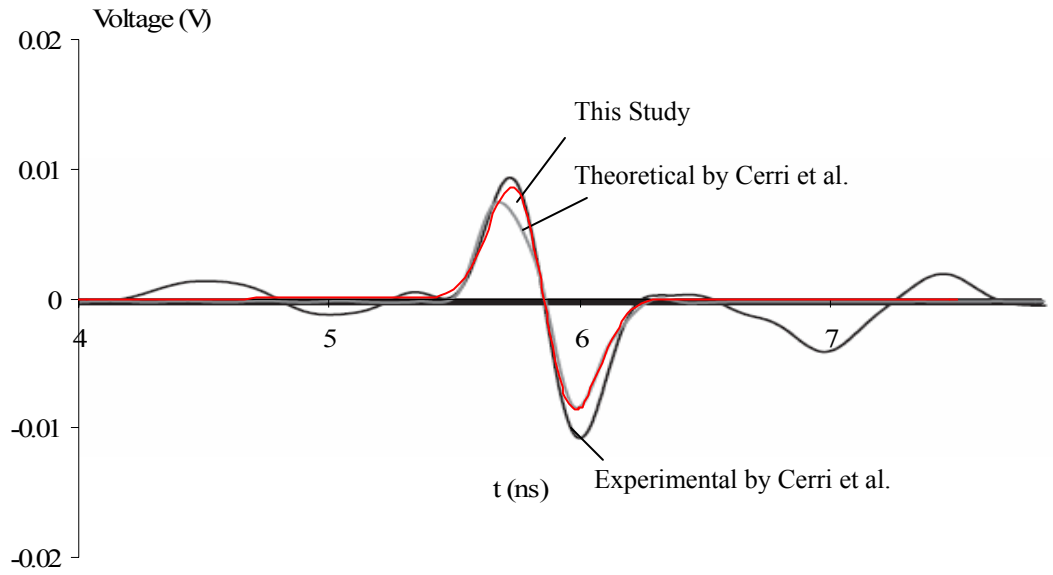

Figure 5.3 Simulated/Tested Reflected Voltage

5.3. COMPARISON WITH MISSOURI S&T TEST DATA

5.3.1. Properties of the Tested Cables. A total of four SR-250C-TA coaxial cables of 1003 mm long each were tested at Missouri S&T. The cross section of each

cable and its dimension are shown in Figures 5.4(a) and 5.4(b). Each cable consists of an outer shield made of TA (Tin-plated Aluminum tube), an inner conductor made of Silver-plated Copper, and a PTFE dielectric layer in between. The characteristic impedance of the cable is 50 Ohm.

(a) Prototype

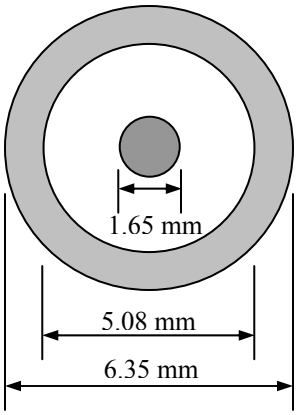

(b) Dimensions

Figure 5.4 Cross Section of the Cables

The four cables tested are divided into two types: Cable 1 and Cable 2. The first three cables, designated as cable 1-1, cable 1-2, and cable 1-3, respectively, are identical three groups of slots were prepared on the surface of the outer conductor, as illustrated in Figure 5.5. Each group has three slots that have the same nominal width and projection length (length perpendicular to the propagation direction) but different inclination angles.

5.3.2. Simulations and Test Results. A step pulse as shown in Figure 5.6 was used in experimentation and simulation. It can be seen that the pulse used in simulation is not exactly the same as the one used in experimentation since the latter does not lead to an analytical solution from the electromagnetic model due to difficulty in

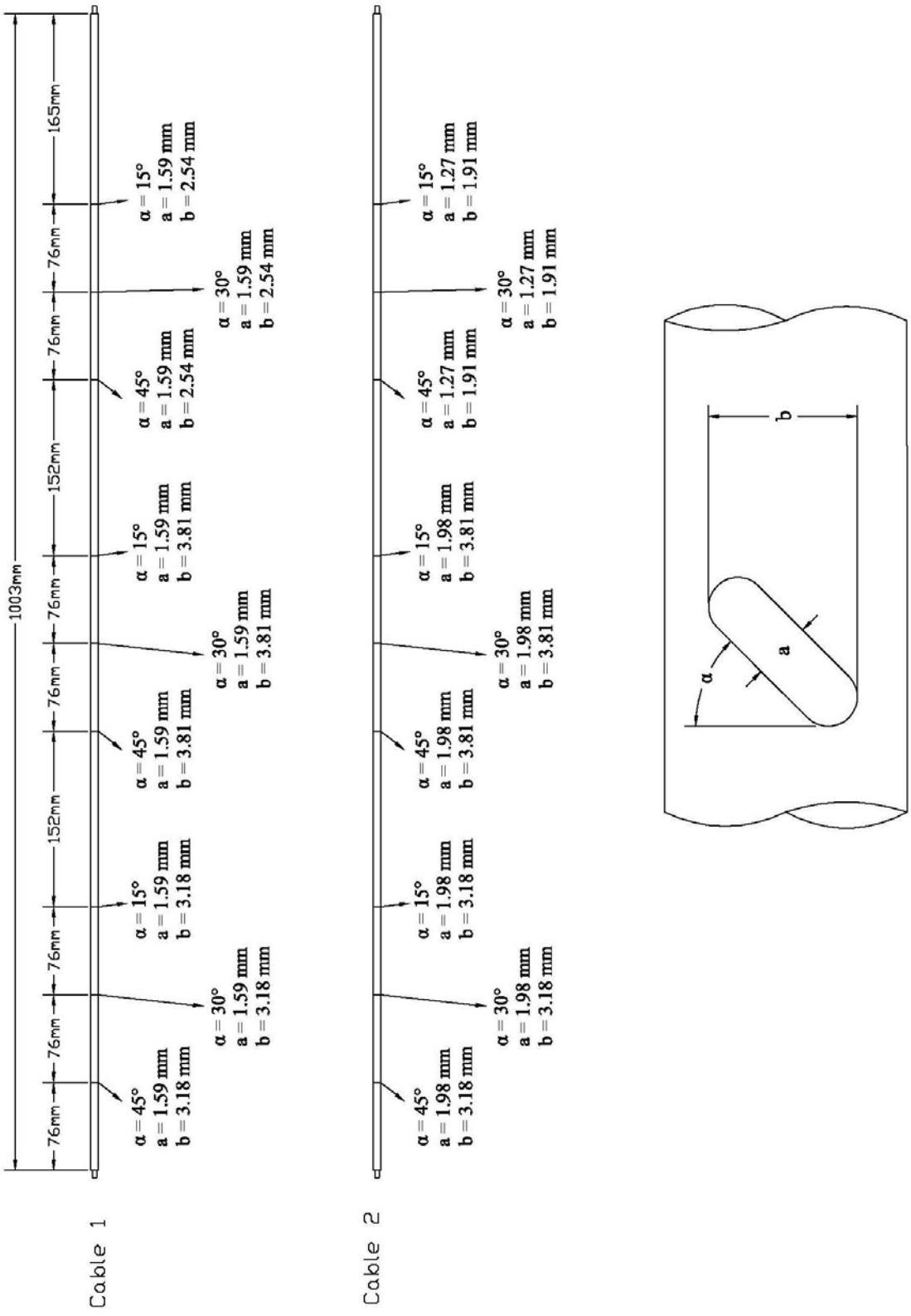

Figure 5.5 Layout of the Slots

Laplace transformation. The overshoot portion of the measured pulse was not taken into account in simulations.

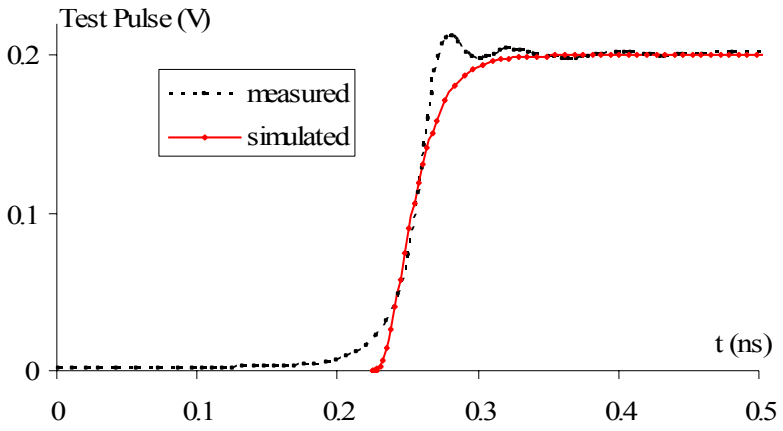

Figure 5.6 Test Pulses Used in Experiment and Simulation

The reflected voltages from cable 1-1, cable 1-2, and cable 1-3 are shown in Figure 5.7. It can be seen from Figure 5.7 that the three measurements are generally consistent except for the second measurement corresponding to the first slot due likely to the partially loosened connection to TDR. As shown in Figure 5.7(a), the reflected voltage waveform from cable 1-3 was shifted to the right side due to imperfect alignment of the slots among the three cables. Except that the two readings from cable 1-1 and cable 1-3 are used for the first slot, the average peak reflected voltage and the range of the three readings at each slot are shown in Figure 5.8 in the form of error bars. Careful examination on Figure 5.8 indicates that, for each group, the variation of three measurements at one slot is larger than the change of their average. Therefore, the effect of inclination angle is unlikely significant even though the average peak value appears decreasing as the inclination angle or the slot length along the cable decreases.

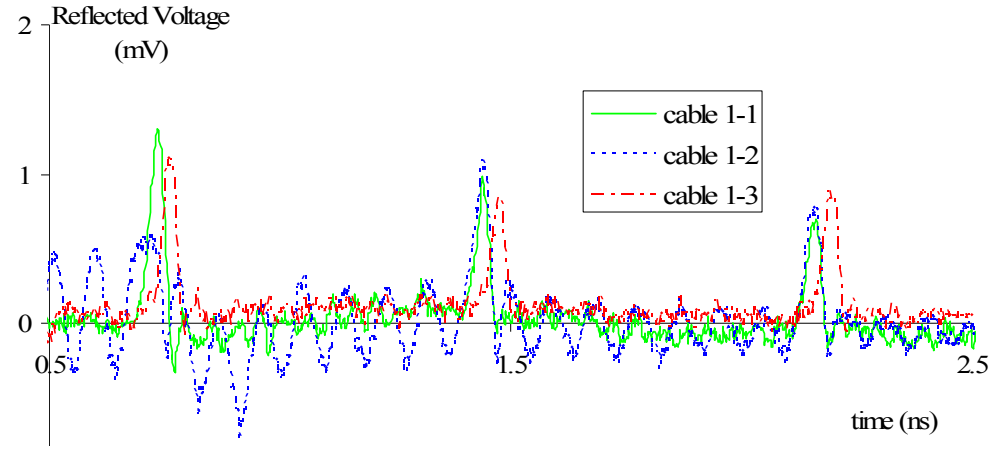

(a) First Group of Slots

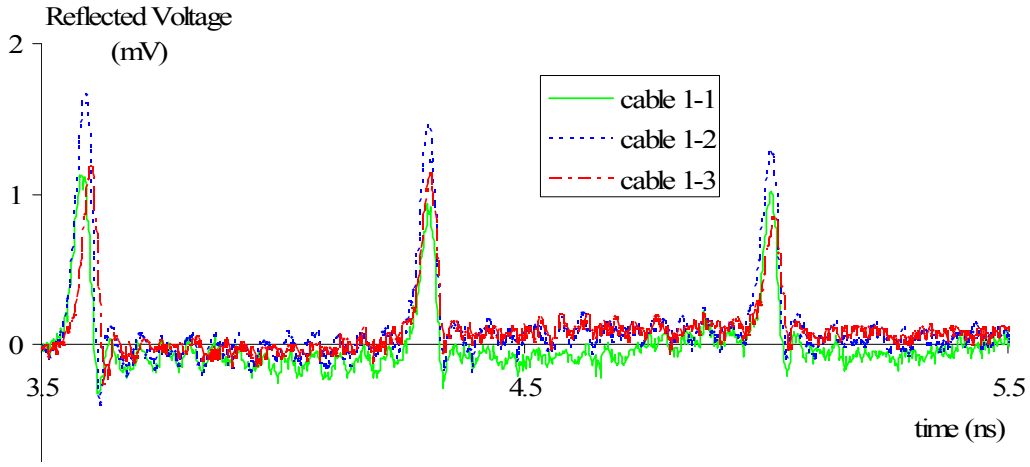

(b) Second Group of Slots

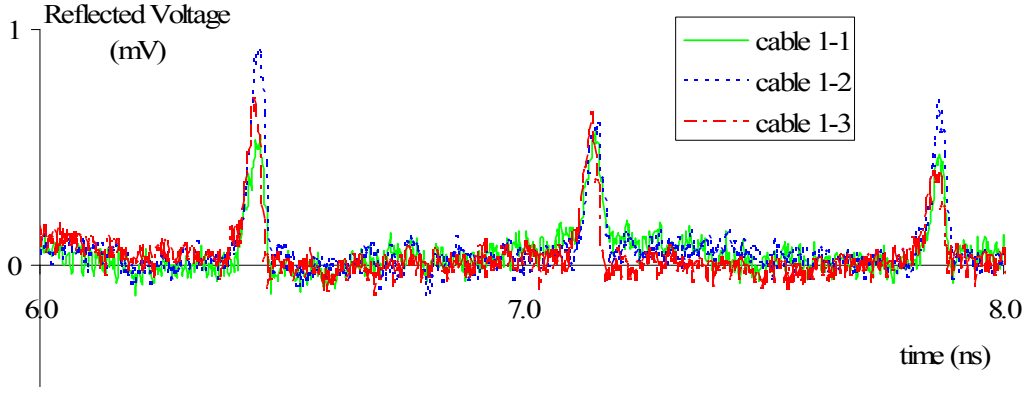

(c) Third Group of Slots

Figure 5.7 Measured Reflected Voltage Waveforms from Cable 1

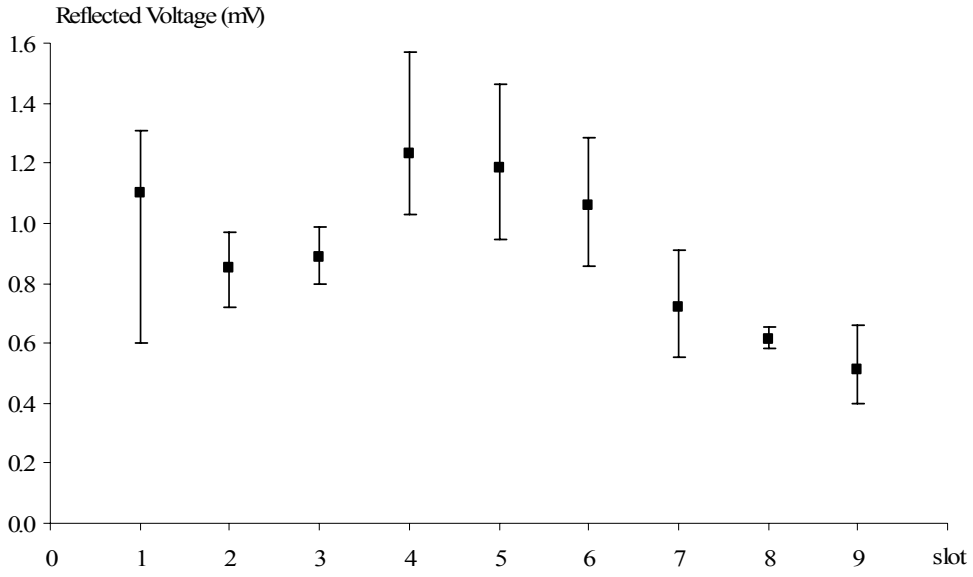

Figure 5.8 Average Peak Voltage and Error Bars for Cable 1

The average of three reflected voltages measured from cable 1-1, cable 1-2, and cable 1-3 is presented in Figure 5.9. Note that the peak values from three measurements were aligned perfectly for each group of slots prior to averaging. The reflected voltage waveform of Cable 2 is shown Figure 5.10. Both figures clearly indicate that the reflected voltages are nearly the same in each group with the same aperture width and projection length. The reflected voltage increases as the projection length (b) of an aperture increases. These features support the conclusions drawn in Section 4.

Both cables were analyzed with the model presented in Section 4. The simulations are compared with the measurements in Figure 5.11 and Figure 5.12 for Cables 1 and 2, respectively. It can be seen that the simulations are in good agreement with the experimental results. The slight difference is mainly attributable to the inaccurate simulation of the test pulse as illustrated in Figure 5.6.

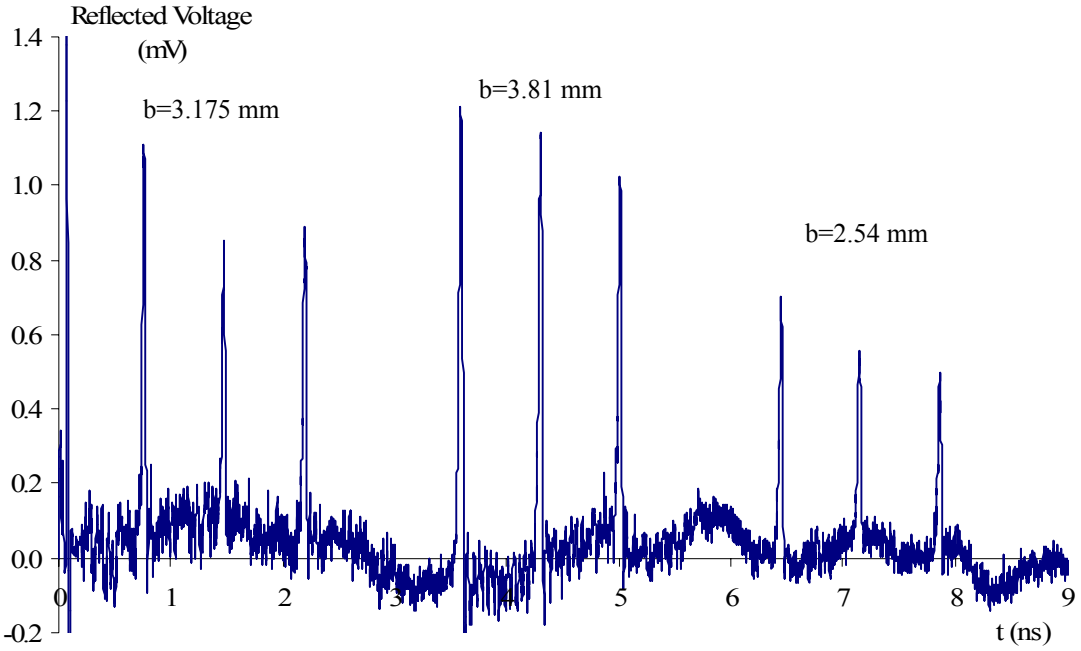

Figure 5.9 Average Reflected Voltage Waveform for Cable 1

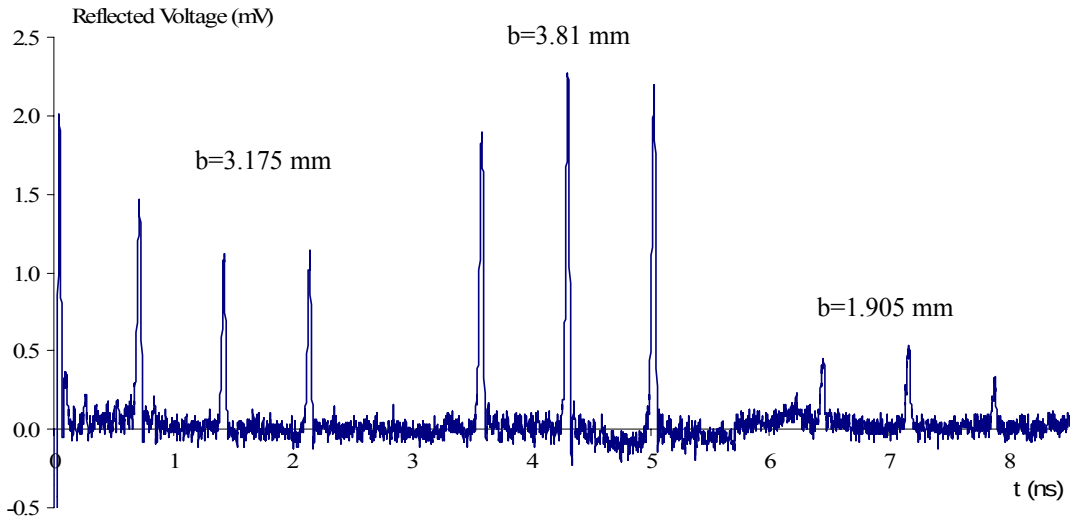

Figure 5.10 Reflected Voltage Waveform for Cable 2

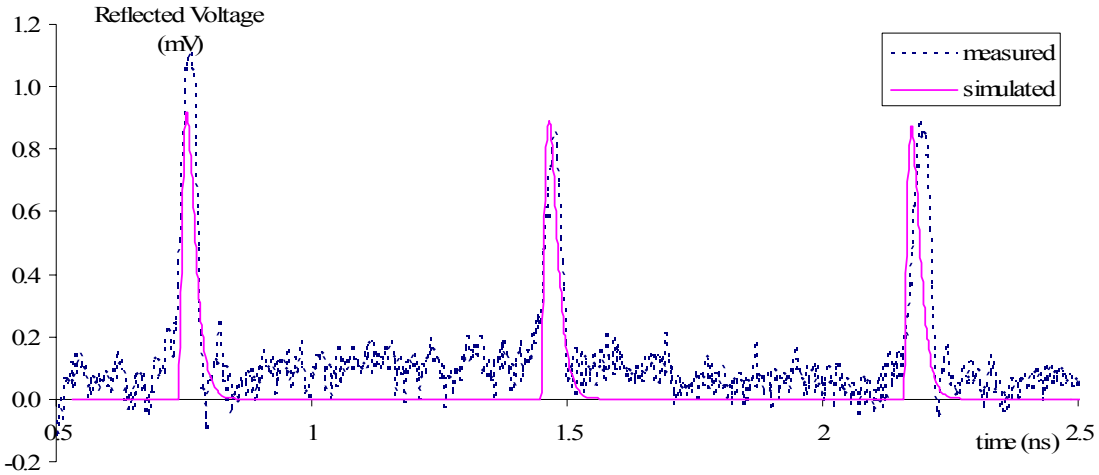

(a) First Group of Slots

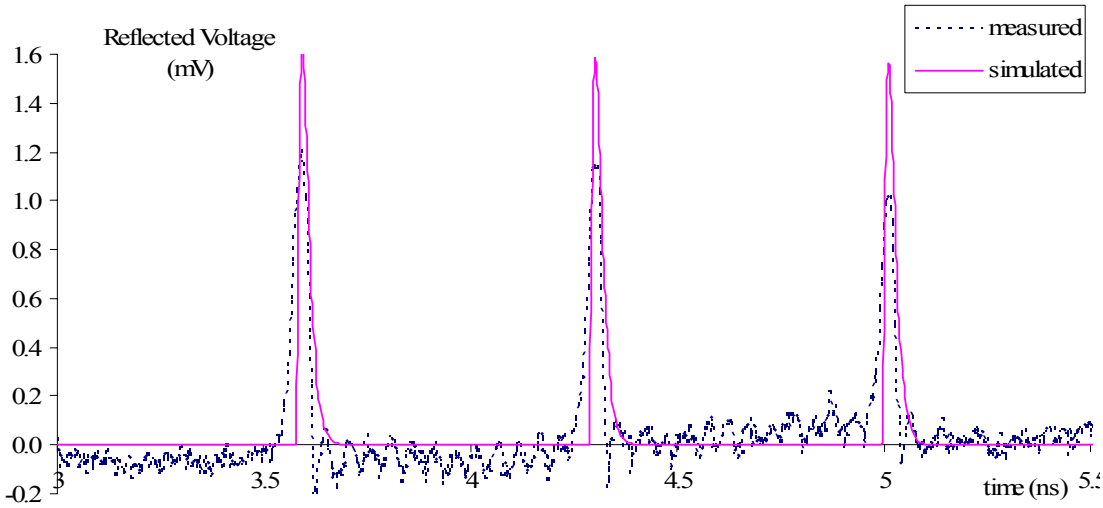

(b) Second Group of Slots

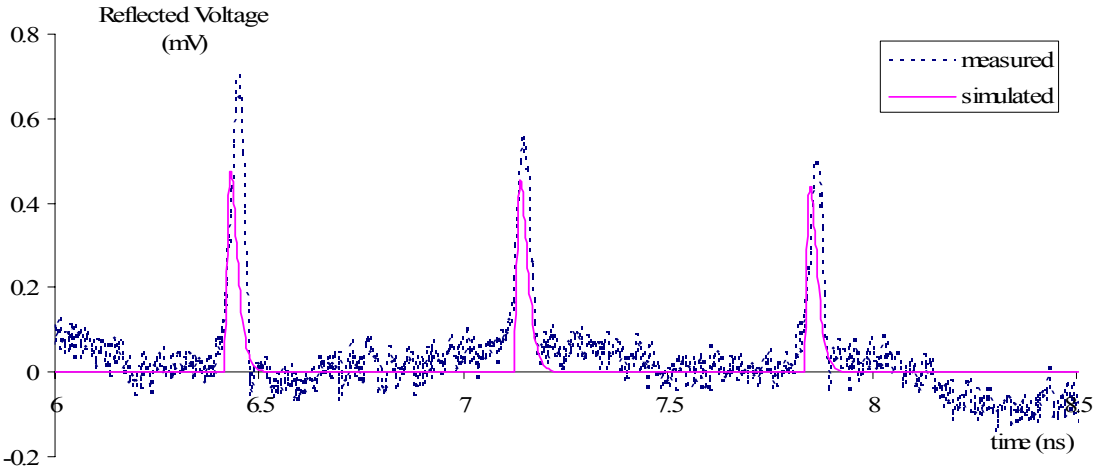

(c) Third Group of Slots

Figure 5.11 Measured / Simulated Reflected Voltages for Cable 1

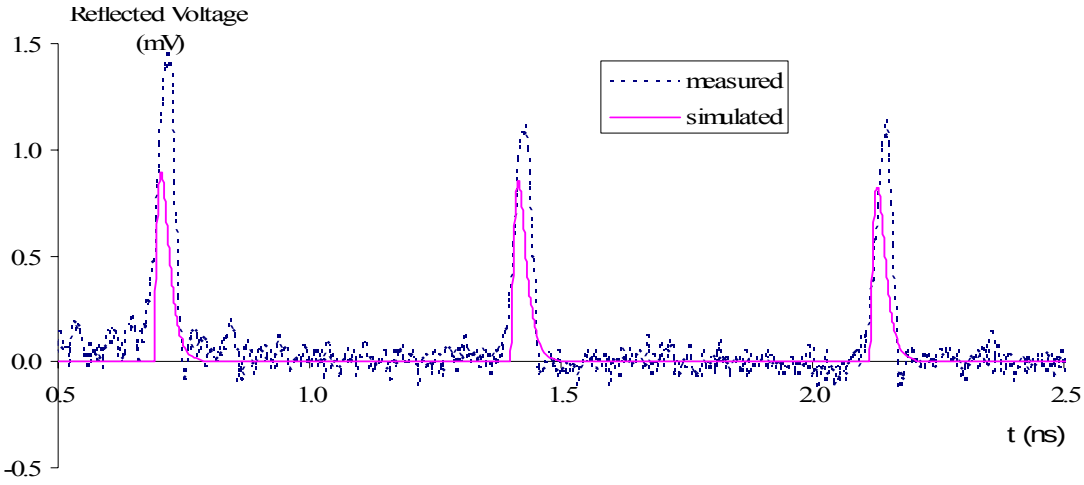

(a) First Group of Slots

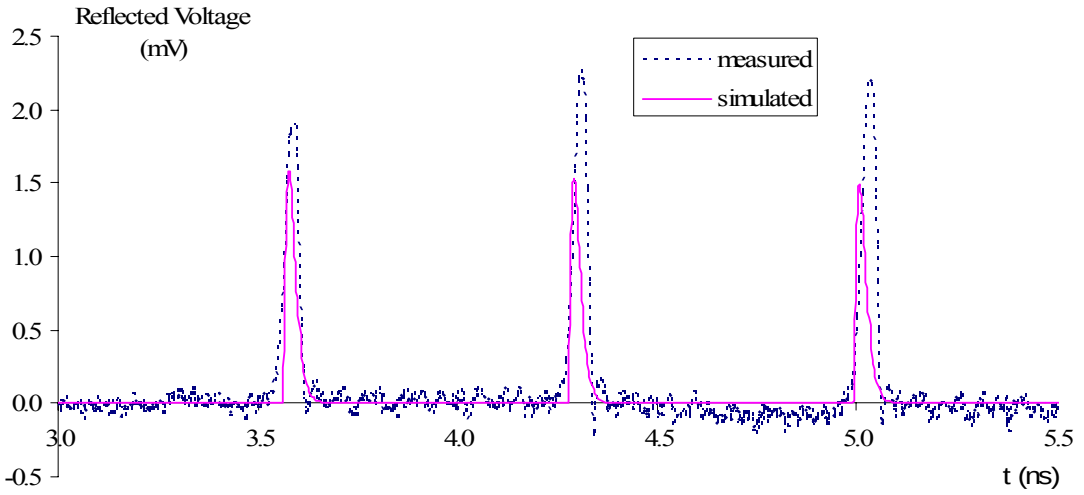

(b) Second Group of Slots

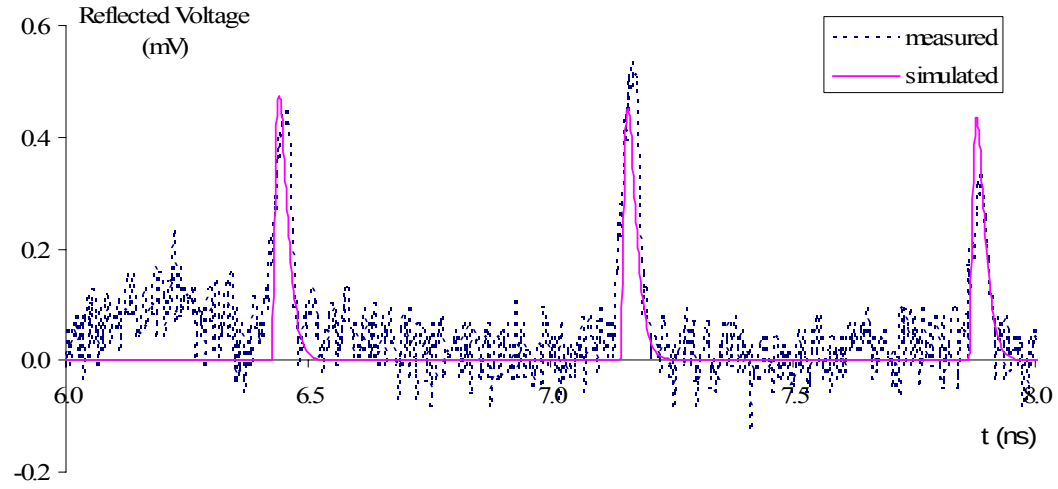

(c) Third Group of Slots

Figure 5.12 Measured / Simulated Reflected Voltages for Cable 2

6. IDENTIFICATION OF LOCAL CONCRETE-SENSOR SLIPPAGES WITH UNCOUPLED ELECTROMAGNETIC AND MECHANICAL MODELING

6.1. INTRODUCTION

Past studies by the Missouri S&T research team have indicated that the soldering layer on the steel spiral of a coaxial cable sensor has a small yet finite strength against strain effects (Mu, 2003). The sensor will thus modify the stress field around it, implying its weak interference on the mechanical modeling of a RC structure. On the other hand, due to strain effects, the steel spiral will separate and leak some of the electromagnetic energy out of the coaxial cable (Sun et al., 2004). This translates into the interference of the mechanical field on the electromagnetic field. However, more recent studies by Brower (2007) verified that such energy release due to strain effects is small since the presence of reinforcing bars will otherwise affect the readings from the cable sensor embedded in concrete. As such, uncoupled electromagnetic and mechanical modeling is considered in this section to approximately represent the concrete-sensor interaction in RC structures.

Simply-supported reinforced concrete (RC) beams are used to show the application of the developed and validated electromagnetic model in Sections 4 and 5. The goal is to identify local concrete-sensor slippages based on the measured reflection coefficient from an embedded cable sensor and the measured crack width in concrete. The key issue in this application is how to model the interface properties between coaxial cable and concrete. For simplicity, the cable-concrete interface is herein assumed to be either perfectly bonded or completely debonded in this study.

6.2. FINITE ELEMENT MODEL

Consider three RC beams of 0.5 m long simply supported at two locations 0.4 m apart, as illustrated in Figure 6.1. To force a single crack to occur at a predetermined location, a 0.25 mm deep and 0.25 mm wide notch is cut at the mid-span of each beam. As shown in Figure 6.2, each beam has a cross section of 63.5 mm × 76.2 mm; it is reinforced by two twisted wires with an equivalent area of 48 mm^2 and instrumented with one embedded cable sensor on the tension side in between two reinforcing bars.

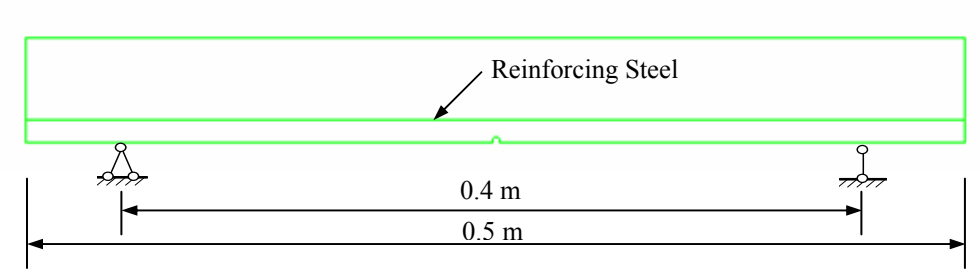

Figure 6.1 Beam Model and Support

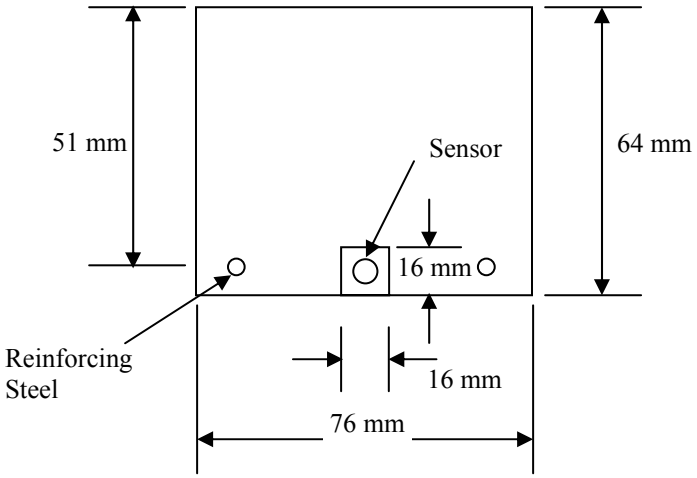

Figure 6.2 Cross Section of the Beam

As shown in Figure 6.3, a two-dimensional (2D) finite element model of a RC beam was set up in DIANA software and evaluated by comparing the results with the

experimental data (Brower, 2007). Under a concentrated load at mid-span, a crack expected to originate and grow along the notch at mid-span. All simulation analyses were performed in displacement control, so that the post-yield behavior can be investigated.

The finite element meshes, the displacement constraints at supports, and the applied load are illustrated in Figure 6.3. The 2D beam model consisted of 304, 8-node quadrilateral elements. Refined meshes were used in the vicinity of the small notch due to stress concentration.

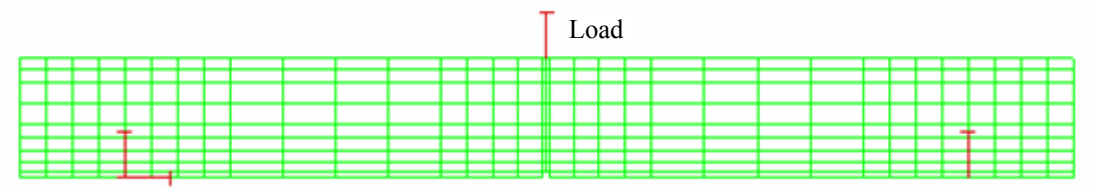

Figure 6.3 2D Model of an RC Beam with Constraints and Load

The compressive and tensile strengths of the concrete were taken to be 25.8 MPa and 2.5 MPa, respectively, based on the cylinder tests (Brower, 2007). The yielding stress and the modulus of elasticity of the reinforcing bars were 413 MPa and 2.0×10^5 MPa, respectively (Brower, 2007). In the 2D model, the concrete behavior was modeled by a parabolic constitutive law. The reinforcing steel behavior was modeled by an elastio-plastic constitutive law.

6.3. CONTROLLED CRACK TEST

To correlate the reflection coefficient from the embedded cable sensor with crack width, a total of ten RC beams were tested at Missouri S&T (Brower, 2007). The

test results of three beams with a single controlled crack are used here to investigate the concrete-sensor interface behavior.

As shown in Figure 6.4, a RC beam was placed upside down for convenience and simply supported at both ends. A concentrated load was applied upward at mid-span to have a so-called three-point bending test. The concentrated load at mid-span was provided by using a car jack at 67 N intervals. A 2.2 kN load cell was used to measure the applied load, and a dial gauge was used to measure the mid-span deflection of the beam. To force the occurrence of a single crack at mid-span of the beam, a pre-cut notch, 0.1 mm wide and 0.1 mm deep, was prepared at the mid-span of each beam. As the crack propagated through the thickness of the beam, the crack width on the surface of each beam was measured with a Peak CS-100 Crackscope.

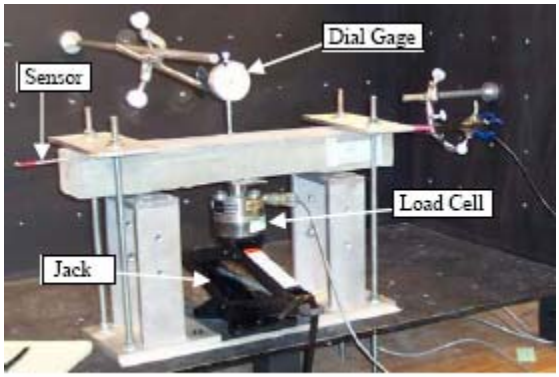

Figure 6.4 Three-point Bending Test of a Simply-Supported Beam

6.4. SIMULATIONS AND TEST RESULTS

The three beams tested in flexure were re-designated as Beam 1 through Beam 3 in this study, corresponding to Beam 3, Beam 4, and Beam 5, respectively, in Brower (2007). The load-deformation curve at mid-span of each beam was simulated and presented in Figure 6.5 when reinforcing bars were perfectly bonded to the concrete. It

can be observed from Figures 6.5 that the beam reached to its ultimate strength at the displacement of 1.8 mm.

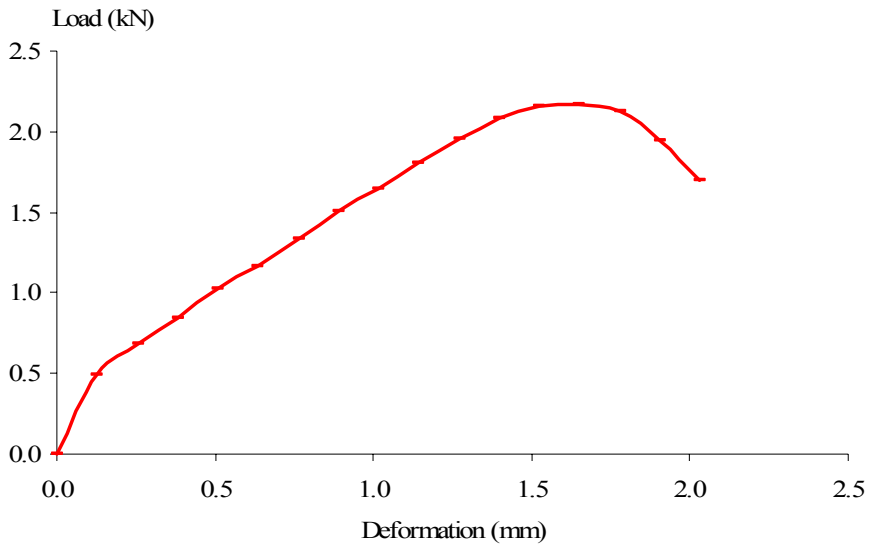

Figure 6.5 Load-deformation Curve at Mid-span

It was observed during tests that crack was originated from the pre-cut notch at the mid-span of the tested beam (Brower, 2007). When the embedded sensor was perfectly bonded to its surrounding concrete, the length of separation between two adjacent steel spiral or the projected length along the wave propagation direction is equal to the crack width in concrete. In this case, the peak reflection coefficient was simulated and plotted against the crack width in Figure 6.6, together with the test data by Brower (2007). In simulations, the length-to-width ratio (L_1/L_2 as illustrated in Figure 4.3) of the aperture on the outer conductor of the sensor is assumed to be 5.

.

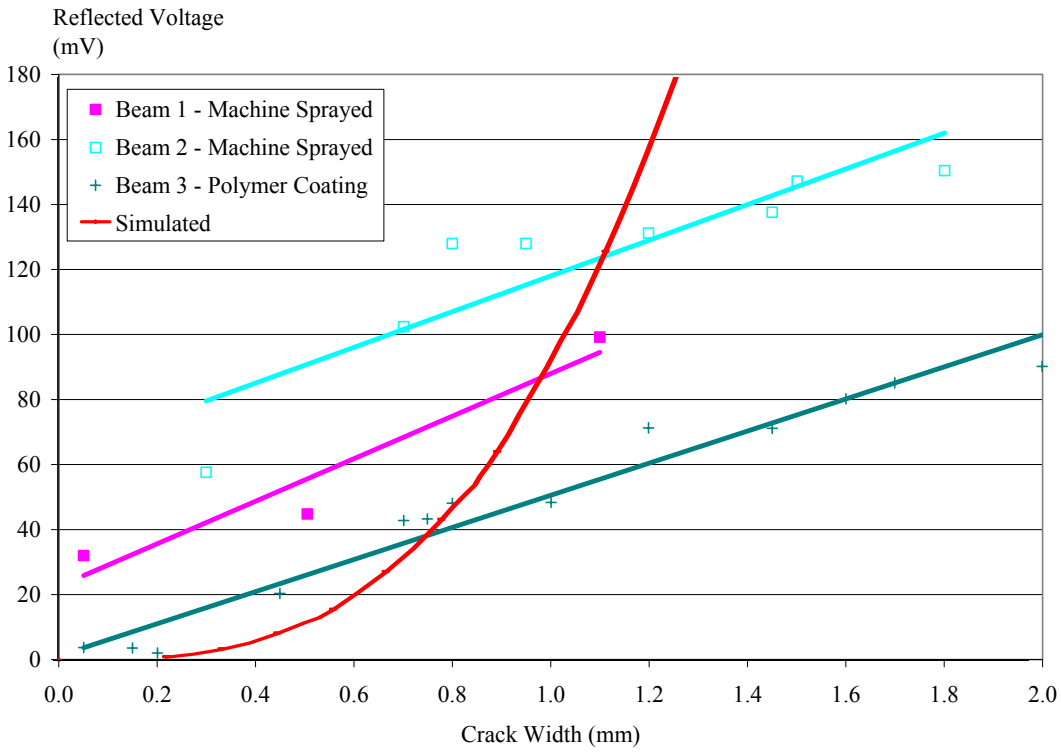

Figure 6.6 Relation between Reflection Coefficient and Crack Width

It can be clearly observed from Figure 6.6 that the correlation between the reflection coefficient and crack width appears parabolic in simulation while it actually is linear according to test data. This difference is most likely attributable to the slippages that have taken place between cable and concrete at the location of cracks. To understand what levels of slippage will lead to a better understanding of the correlation curve, the relation between the length of separation in sensor (or the projected slot width along the propagation direction) and crack width in concrete was identified to make the simulated results consistent with the test data. As shown in Figure 6.7, such a relation indicates that the progression rate of the slot width in sensor is approximately 1/4 of that of the corresponding crack width in concrete. Considering the width of steel spiral used in the fabrication of coaxial cable sensors, this relation seems reasonable. Note that the aperture

length identified in simulations, L_1 in Figure 4.3, range from 1.3 mm to 2.4 mm, corresponding to test data.

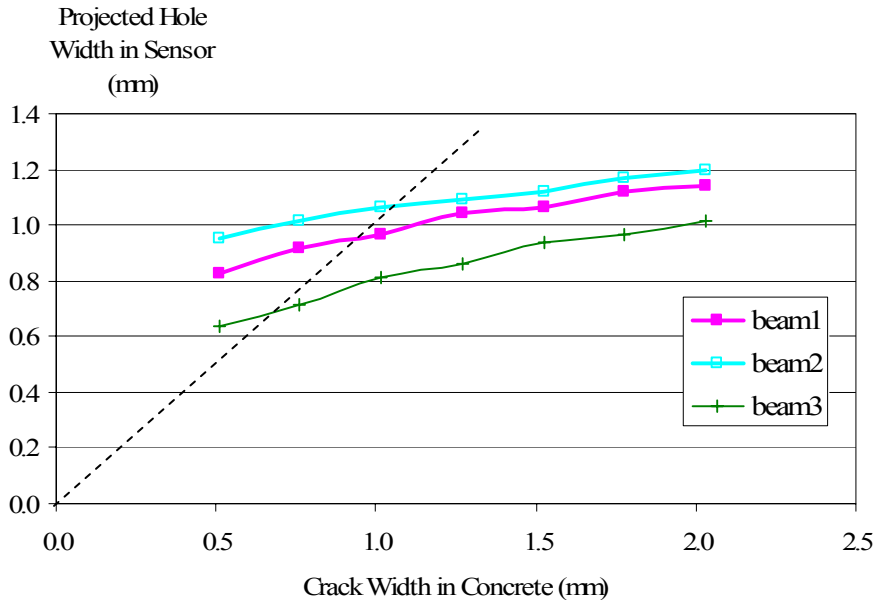

Figure 6.7 Projected Slot Width in Sensor vs. Crack Width in Concrete

A dash line is also shown in Figure 6.7 to represent the perfectly bonded case between concrete and sensor. It is seen from Figure 6.7 that, for all three beams modeled, a small portion of the relation between the projected slot width in sensor and crack width in concrete implies that the projected slot width is even larger than that in crack width. This portion of simulations seems inaccurate. Closer examinations on the test data in Figure 6.6 reveal that the inaccuracy modeling in this range is closely related to the finite strength of the soldering layer of the sensor, which is not taken into account in the current simulations.

Based on the results shown in Figure 6.7, the slippage of concrete over the embedded sensor can be evaluated and presented in Figure 6.8. This figure further indicates that, at small crack width, the slippage is negative, which is unrealistic.

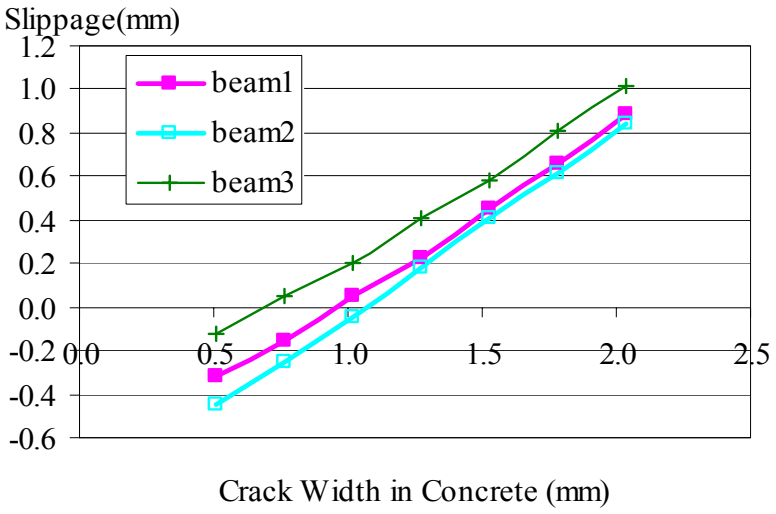

Figure 6.8 Slippage vs. Crack Width in Concrete

6.5. SUMMARY

A RC beam with a small notch at mid-span was simulated in DIANA software. The simulation results were compared with those acquired from controlled crack tests. When the embedded sensor is perfectly bonded to its surrounding concrete, the reflection coefficient is related to the crack width in concrete in parabolic form, which differs from the linear relation observed from test data. When the progression rate of slot width in sensor is assumed to be ¼ of corresponding crack width in concrete, the reflection coefficient is in excellent agreement with the crack width in concrete according to the test data. Therefore, the slippage between concrete and sensor can be approximated to be the difference between the projected slot width and the concrete width.

7. CONCLUSIONS

Coaxial cable sensors, once embedded to RC structures, can detect cracks in concrete since cracks are transferable to coaxial cables in the form of apertures on the surface of their outer conductor. As such, it is critically important to locate and identify apertures in coaxial cables. The model proposed in this study has been limited to the application of a square aperture by others. This study has extended the model to study defects of any shape and applied it into RC beams to understand concrete-sensor interface behaviors.

In this thesis, small elliptical apertures/slots on a coaxial cable have been modeled with the electromagnetic wave theory to estimate the reflection they produce on impinging test signals. In this way it is possible to assess the sensitivity of TDR techniques in detecting the presence and location of faults on cables. The theoretical results were validated by experimental measurements and full wave simulation results. The model was also applied to RC beams to identify the slippage between concrete and embedded sensor.

Future studies should be directed to a better modeling of the input pulse used during the tests at Missouri S&T so that more details of the test results can be simulated with the model developed in this study. Particularly, both peak and width of the reflected pulse can be further examined to better understand the sensitivity and spatial resolution of sensors as well as signal loss. More importantly, a coupled electromagnetic and mechanical model must be developed to understand the effects of the soldering layer strength in sensors on the sensor sensitivity and general performance.

BIBLIOGRAPHY

Benson, C. H. and Bosscher, P. J. (1999), "Time-domain reflectometry (TDR) in geotechnics: a review," *Nondestructive and Automated Testing for Soil and Rock Properties*. ASTM STP 1350, W.A. Marr and C.E. Fairhurst, Eds, American Society for Testing and Materials, West Conshohocken.

Brower, M. A., (2007), "Implementation issues of distributed coaxial cable crack sensors embedded in reinforced concrete members," *M.S. Thesis*, University of Missouri-Rolla, Rolla, MO.

Brower, M. A., Royer, Z. L., Chen, G. D., Van Aken, D. C., Pommerenke, D. (2006),"Distributed Cable Sensors for Structural Damage Detection: Implementation Issues,"*Proceedings of the 2006 ASCE Structural Congress,* St. Louis, May 18-20.

Cerri, G., De Leo, R., Della Nebbia, L., Pennesi, S., Mariani Primiani, V. and Russo P. (2005), "Fault location on shielded cables: Electromagnetic modelling and improved measurement data processing," *IEE Proceeding-Science, Measurement and Technology*, Vol. 152, No. 5, September 2005.

Chen, C.S., and Loemer, L.E. (1976), "The application of cepstrum technique in power cable fault detection," *IEEE International Conference on ICASSP(Acoustic, Speech and Signal Processing)*, Apr. 1976, Vol. 1, pp. 764 – 767

Chen, G. D., Sun, S. S., Pommerenke, D., Drewniak, J. L., Greene, G. G., McDaniel, R. D., Belarbi, A., and Mu, H. M. (2003), "Crack detection of a 15 meter long reinforced concrete girder with a single distributed cable sensor," *Proceedings of 1st International Conference on Structural Health Monitoring and Intelligent Infrastructures,* Tokyo, Japan, November 2003.

Chen, G. D. (2004), "Development and validation of novel distributed coaxial cable sensors for crack detection," *Proceedings of 3rd Sino-Japan-US Symposium on Structural Health Monitoring and Control*, Dalian, China, October 2004.

Chenaf, D., and Amara, N. "Time domain reflectometry for the characterization of diesel contaminated soils," *Second International Symposium and Workshop on Time Domain Reflectometry for Innovative Geotechnical Applications*, Northwestern University, Evanston, Illinois, 2001.

Collin, R. E.,"Foundations for microwave engineering" (McGraw Hill International Editions, Singapore, 1992)

Comoda, M., Kawashima, T., Arakane, M., Aihara, M., Fujiwara, Y., and Shinagawa, J. (1991) "Development of a current detection type fault locator," *IEEE Transactions On Power Delivery*, 1991, 6, pp. 541 – 545

De Meulenaere, F. and Van Bladel, J. (1977), "Polarizability of Some Small Apertures," *IEEE Transactions on Antennas and Propagation*, Vol. AP-25, No. 2, March 1977

Iskander, M. F. (1992), "Elctromagnetic fields and waves" (Prentice Hall, Englewood Cliffs, NJ, 1992)

Mu, H. M., (2003), "Development and validation of coaxial cable sensors for damage detection of reinforced concrete structures," *Ph.D. Dissertation*, University of Missouri-Rolla, Rolla, MO.

McDaniel, R. D., (2004), "Characterization and implementation of distributed coaxial cable sensors for embedment in reinforced concrete structural members," *M.S. Thesis*, University of Missouri-Rolla, Rolla, MO.

Lin, M. W., Abatan, A. O., and Zhang, W. (1998), "Crack damage detection of concrete structures using distributed electrical time domain reflectometry (ETDR) sensors," *Proceedings of 5th SPIE Annual Symposium on Smart Structures and Materials: Smart Systems for Bridges, Structures, and Highways*, Vol. 3325, Newport Beach.

Lin, M. W., Abatan, A. O., and Zhou, Y. (2000), "High sensitivity electric TDR distributed strain sensor," *Proceedings of 7th SPIE Annual Symposium on Smart Structures and Materials 2000: Smart Systems for Bridges, Structures, and Highways*, Vol. 3986, Newport Beach, March 2003.

Nawy, E. G. (2003), *Reinforced Concrete: a Fundamental Approach*, 5th Edition, Prentice Hall, Upper Saddle River, NJ.

O'Connor, K. M., Peterson, D. E., and Lord, E. R. "Development of a highwall montoring system using Time Domain Reflectometry," *Proceedings of the 35th U. S. Symposium on Rock Mechanics*, Reno, Nevada, 1995.

Okanla, E. I., Gaydecki, P. A., Manaf, S., and Burdekin, F. M. "Detecting faults in posttensioning ducts by electrical time-domain reflectometry," *Journal of Structural Engineering – ASCE*, Vol. 123, No. 5, p. 567-574, May 1997.

Sun, S. S., Pommerenke, D., Drewniak, J. L., and Chen, G. D. (2004), "Signal loss, spatial resolution, and sensitivity of long coaxial crack sensors," *Proceedings of 11th SPIE Annual Symposium on Smart Structures and Materials*, San Diego, March.

Van Bladel, J. (2007), "Electromagnetic fields," Wiley-Interscience Inc.

VITA

Mei Wang was born on May 21, 1975 in Jiangsu, China. In July of 1998, she received her Bachelor of Science Degree in Structural Engineering from Tsinghua University, P.R. China. She received her Doctor of Philosophy Degree in Structural Engineering in January 2003 from Tsinghua University, P.R. China. Mei began her graduate study at the University of Missouri – Rolla in January of 2006. She received a Master of Science Degree in Civil Engineering in May 2008 from the Missouri University of Science and Technology (formerly University of Missouri-Rolla).